

# Production of renewable jet fuel range alkanes and commodity chemicals from integrated catalytic processing of biomass

Cite this: *Energy Environ. Sci.*, 2014, 7, 1500

Jesse Q. Bond,<sup>a</sup> Aniruddha A. Upadhye,<sup>b</sup> Hakan Olcay,<sup>c</sup> Geoffrey A. Tompsett,<sup>d</sup> Jung-ho Jae,<sup>e</sup> Rong Xing,<sup>f</sup> David Martin Alonso,<sup>b</sup> Dong Wang,<sup>b</sup> Taiying Zhang,<sup>g</sup> Rajeev Kumar,<sup>g</sup> Andrew Foster,<sup>h</sup> S. Murat Sen,<sup>b</sup> Christos T. Maravelias,<sup>b</sup> Robert Malina,<sup>c</sup> Steven R. H. Barrett,<sup>c</sup> Raul Lobo,<sup>h</sup> Charles E. Wyman,<sup>gi</sup> James A. Dumesic<sup>b</sup> and George W. Huber<sup>\*b</sup>

This article presents results from experimental studies and techno-economic analysis of a catalytic process for the conversion of whole biomass into drop-in aviation fuels with maximal carbon yields. The combined research areas highlighted include biomass pretreatment, carbohydrate hydrolysis and dehydration, and catalytic upgrading of platform chemicals. The technology centers on first producing furfural and levulinic acid from five- and six-carbon sugars present in hardwoods and subsequently upgrading these two platforms into a mixture of branched, linear, and cyclic alkanes of molecular weight ranges appropriate for use in the aviation sector. Maximum selectivities observed in laboratory studies suggest that, with efficient interstage separations and product recovery, hemicellulose sugars can be incorporated into aviation fuels at roughly 80% carbon yield, while carbon yields to aviation fuels from cellulose-based sugars are on the order of 50%. The use of lignocellulose-derived feedstocks rather than commercially sourced model compounds in process integration provided important insights into the effects of impurity carryover and additionally highlights the need for stable catalytic materials for aqueous phase processing, efficient interstage separations, and intensified processing strategies. In its current state, the proposed technology is expected to deliver jet fuel-range liquid hydrocarbons for a minimum selling price of \$4.75 per gallon assuming  $n^{\text{th}}$  commercial plant that produces 38 million gallons liquid fuels per year with a net present value of the 20 year biorefinery set to zero. Future improvements in this technology, including replacing precious metal catalysts by base metal catalysts and improving the recyclability of water streams, can reduce this cost to \$2.88 per gallon.

Received 25th November 2013  
Accepted 3rd February 2014

DOI: 10.1039/c3ee43846e

[www.rsc.org/ees](http://www.rsc.org/ees)

## Broader context

This article summarizes outcomes from a collaborative research program that integrated biomass pretreatment and chemical conversion strategies to deliver commodity chemicals and surrogate aviation fuels directly from hardwoods. A major concern in commercialization of biomass conversion strategies is process integration and the extent to which strategies developed at bench scales for upgrading model compounds can be translated into practical applications using actual biomass. Biomass refining strategies are inherently complex, and selective transformations of lignocellulose constituents (*e.g.*, sugars) into targeted products requires fractionation such that each component is recovered individually and optimally utilized according to its chemical and physical properties. Here, we demonstrate the integration of multiple biomass processing technologies and examine the impact of employing a realistic lignocellulose source in the production of industrial commodities. This integrated strategy provides a potential roadmap for the production of lignocellulosic aviation fuels, which are of long-term, strategic importance. We additionally present an economic analysis of the technology, establishing that the approach could provide an economically viable alternative as petroleum supplies diminish. Furthermore, based on both experimental research and process modelling and analysis, we outline key research needs in the production of aviation fuels from abundant biomass.

<sup>a</sup>Department of Biomedical and Chemical Engineering, Syracuse University, Syracuse, New York, 13244, USA

<sup>b</sup>Department of Chemical and Biological Engineering, University of Wisconsin–Madison, Madison, Wisconsin, 53706, USA. E-mail: [huber@enr.wisc.edu](mailto:huber@enr.wisc.edu)

<sup>c</sup>Laboratory for Aviation and the Environment, Department of Aeronautics and Astronautics, Massachusetts Institute of Technology, Cambridge, MA, 02139, USA

<sup>d</sup>Department of Chemical Engineering, Worcester Polytechnic Institute, Worcester, MA, 01609, USA

<sup>e</sup>Korea Institute of Science and Technology, Seoul 136-791, Republic of Korea

<sup>f</sup>Department of Chemical Engineering, University of Massachusetts–Amherst, Amherst, Massachusetts, 01003, USA

<sup>g</sup>Center for Environmental Research and Technology (CE-CERT), Bourns College of Engineering, University of California, Riverside, CA, 92521, USA

<sup>h</sup>Department of Chemical and Biomolecular Engineering, University of Delaware, Newark, Delaware, 19716, USA

<sup>gi</sup>Department of Chemical and Environmental Engineering, Bourns College of Engineering, University of California, Riverside, CA, 92521, USA

# 1 Introduction

Establishing energy security in the face of diminishing fossil reserves is an essential requirement for sustainable development of society. Within this context, a continued supply of hydrocarbon fuels is a primary challenge since the transportation sector is the largest single consumer of crude oil.<sup>1</sup> In 2010, the United States processed a total of 7 billion barrels of petroleum, with 71% of petroleum going toward meeting a combined demand of 5.2 billion barrels of gasoline, jet, and diesel fuels.<sup>2</sup> Even without considering projected increases in liquid fuel consumption, the future availability of crude oil is uncertain.<sup>3</sup>

A more sustainable approach will replace petroleum in the transportation sector with renewable alternatives as stipulated in the Energy Independence and Security Act, which mandates that 36 billion gallons (857 million barrels) of renewable fuels be blended annually into the liquid transportation fuel infrastructure by 2022.<sup>4</sup> Currently, the US uses about 14 billion gallons of renewable fuels, majority of which are supplied by corn ethanol or triglyceride-based biodiesel.<sup>2</sup> Unfortunately, starches and triglycerides cannot be produced at a sufficient scale to annually supply 36 billion gallons of renewable transportation fuels, and it is clear that new technologies leveraging more abundant carbon sources must come to market. Because of its broad availability, lignocellulose is considered the most appropriate long-term alternative to fossil carbon.<sup>5</sup> A 2011 study estimates that the United States can sustainably deliver 1.6 billion tons of lignocellulose per year.<sup>6</sup> With proper technological advances, this could offset 43% of the total domestic petroleum consumption or 58% of the petroleum currently used in producing transportation fuels, easily clearing mandated targets. However, a large-scale transition to lignocellulosic fuels is constrained by economic and technical challenges associated with converting woody biomass into “drop-in” fuels.

Renewably sourced oxygenates have historically been the primary biofuel targets, such as ethanol and butanol intended for gasoline blending. However, the large-scale utility of oxygenated fuels is limited by their reliance on sugar monomer isolation (*e.g.*, obtaining glucose from cellulose), low yields, difficult separations, high costs, or poor compatibility with existing infrastructure. For example, ethanol<sup>7</sup> and butanol<sup>8</sup> can be produced efficiently by microbial fermentation of lignocellulosic sugars, but their blending is restricted in gasoline engines. Other fuel-grade oxygenates include mixed mono-functionals,<sup>9–11</sup> levulinate esters,<sup>12–14</sup>  $\gamma$ -valerolactone (GVL),<sup>15–19</sup> and 2-methyltetrahydrofuran (MTHF).<sup>20,21</sup> These can all be prepared through aqueous phase, chemical conversion of carbohydrates and thus appear industrially attractive; however none are currently available as commercial scale fuel additives. Additionally, the low volumetric energy density of oxygenates prohibits their inclusion in aviation fuels. This is a concern since current projections indicate that the demand for distillate fuels in the US will continue to increase over the next 20 years while the demand for gasoline—for which oxygenates are a suitable analog—will decrease. Demand for gasoline in the US

is projected to decrease by 22% by the year 2040 thanks to the improved efficiency in gasoline vehicles and electric vehicles.<sup>22</sup> However, demand for diesel and jet fuel is expected to continue to increase by 27% in the next few years.<sup>22</sup> Although near-term production of oxygenates will aid in meeting renewable fuel mandates through gasoline blending (*i.e.*, 36 billion gallons by 2022 (ref. 4)), it is essential to shift biofuel production toward distillate-range liquid alkanes in the long term. This will permit lignocellulosic carbon to supply energy-dense hydrocarbons in essential sectors while technological advances enable increasing use of alternative power for light-duty transportation.<sup>23,24</sup>

The most well-developed strategies for the production of bio-derived jet fuel are lignocellulose gasification followed by Fisher–Tropsch Synthesis (FTS) and triglyceride hydrodeoxygenation.<sup>25</sup> FTS is effective for producing liquid fuels from coal and natural gas; however, it may not be appropriate for biomass conversion since FTS plants are capital intensive and thus necessitate centralized processing in large facilities. Gasification-based technologies will therefore incur additional expenses associated with transporting low energy density biomass over relatively large distances. Other challenges with lignocellulose gasification include feeding biomass particles into pressurized reactors, expensive oxygen plants, and fouling of process equipment due to tar formation. Triglyceride-based strategies are efficient and can produce high-quality distillate fuels though decarbonylation, decarboxylation, and hydrogenation, but they are constrained by the cost and availability of triglycerides from either oil-producing plants or algae. These issues warrant a shift toward distributed-scale technologies that efficiently leverage lignocellulose. Although bench scale research has demonstrated the possibility of producing liquid alkane fuels from woody biomass,<sup>26–30</sup> reported strategies have been predominately optimized to leverage only cellulose. Frequently, minor components are underutilized, decreasing the industrial viability of lignocellulose processing. Consequently, lignocellulosic biofuels are more expensive to produce than petroleum-derived fuels.<sup>31</sup> To ensure maximal carbon yields and permit cost effective operation, biorefineries must simultaneously offer value-added conversion of hemicellulose and lignin. Given the unique chemical and physical properties of lignocellulose components, an economically feasible lignocellulose-to-fuels process will likely require a multi-faceted approach (*e.g.*, a combination of hydrolysis and pyrolysis) through which each biomass fraction is leveraged appropriately to deliver maximal carbon yields to desired products. To facilitate the design of an integrated biorefinery, it is also important that current research address practical aspects of technology translation and scale up that arise when integrating multiple biomass conversion technologies.

To this end, we present an integrative approach toward the production of jet fuel components and commodity chemicals from hardwood feedstocks. The objective of this work is to address the conversion of whole lignocellulose to C<sub>8</sub> and larger hydrocarbon fuels with maximum overall carbon yield using stable, catalytic processes with residence times below 1 hour. Bench scale laboratory studies were combined with economic

modelling to develop a practical, cost effective approach for the production of liquid alkanes from lignocellulose. We have observed that a combination of technologies based upon carbohydrate hydrolysis can deliver “drop-in” aviation fuels alongside chemical co-products, such as acetic acid. Additionally, efficient management of contaminants and residuals is critical to achieving stable catalyst performance, good selectivities, and viable product yields.

## 2 Technology overview

Fig. 1 summarizes the integrated, catalytic process envisioned here. At the outset of the program, research efforts explored both direct, thermochemical conversion of whole biomass and hydrolytic fractionation for production of a hydrocarbon mixture intended to match the specifications of jet propellant 8 (JP-8). Ultimately, hydrolysis-based strategies were found to be more efficient in targeted jet fuel production since they allow high carbon yields and selective processing of C<sub>5</sub> and C<sub>6</sub> sugars to produce linear and branched alkanes. Though studies reported here were performed with red maple or mixed hardwoods, the overall process is adaptable to many lignocellulosic feedstocks, particularly those rich in xylans (e.g., miscanthus, switchgrass, or poplar). The remainder of this section provides a general synopsis of the technology platform illustrated by Fig. 1.

Lignocellulose is first pretreated using hot water extraction (autohydrolysis). Dilute acid hydrolysis with either H<sub>2</sub>SO<sub>4</sub> or oxalic acid are also viable pretreatment options; however, the particular applications here are best suited to hot water extraction. Through hot water pretreatment, 85% of hemicellulose sugars are recovered as an aqueous solution of

xylooligomers.<sup>32</sup> Hemicellulose oligomers are subsequently introduced to a two-stage, biphasic reactor along with HCl and tetrahydrofuran (THF). In the first stage, hemicellulose oligomers are hydrolyzed to form a mixture of sugars—predominately xylose—as well as organic acids. In the second stage, sugar monomers are dehydrated to form furans. Furfural is produced *via* xylose and arabinose dehydration in excess of 90% carbon yield and is recovered in the THF extracting phase alongside acetic acid.

Both acetic acid and furfural can be sold in commodity chemical markets; however, since this approach targets aviation fuel production, furfural is used as a platform for synthesis of long-chain alkanes.<sup>33</sup> Specifically, furfural is condensed in basic media, with an acetone co-feed, to produce high molecular weight oxygenates (C<sub>7</sub>–C<sub>31</sub>) in good carbon yields (>90%).<sup>30</sup> These oxygenates are then processed over bifunctional catalysts, along with a hydrogen co-feed, to fully remove oxygen and saturate any C=C bonds, improving energy density and stability.<sup>34</sup> The end product of furfural upgrading is thus a blend of straight-chain and branched alkanes that retain the majority of the carbon contained in the parent sugar molecules.

Pretreated solids, comprised of cellulose and lignin, are recovered from hot water autohydrolysis and are subsequently treated with dilute sulfuric acid (H<sub>2</sub>SO<sub>4</sub>) using a stirred tank reactor or a steam-gun. In this manner, cellulose is converted to levulinic (LA) and formic acids (FA) at 75% of the maximum theoretical molar yield. LA and FA are recovered in aqueous solution along with the sulfuric acid catalyst. Residual solids from this step contain lignin and degradation products, which form during hydrolysis through parallel pathways. Solids, recovered by filtration, are then used as a boiler feed for process

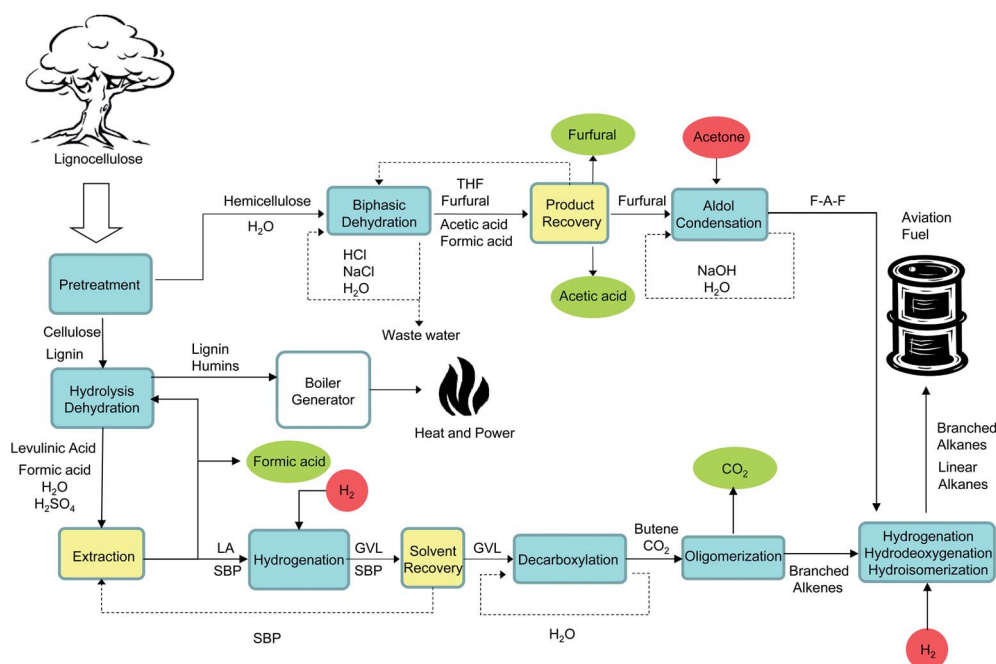


Fig. 1 Conceptual overview of proposed technology for the production of furfural, jet fuels, and acetic acid from lignocellulose. Abbreviations: FAF, furfural–acetone–furfural; GVL,  $\gamma$ -valerolactone; SBP 2-secbutyphenol; LA, levulinic acid; THF, tetrahydrofuran.

heat. LA is recovered from the hydrolyzate *via* extraction using 2-secbutylphenol (SBP) and is subsequently converted, without separation, to  $\gamma$ -valerolactone (GVL) by hydrogenation over a RuSn/C catalyst (>95% carbon yield).<sup>35,36</sup> Multiple extraction/hydrogenation cycles can be optionally employed to increase the GVL concentration and improve the energy efficiency of GVL recovery. GVL is then further converted to branched, C<sub>8</sub>–C<sub>16</sub> alkenes in a two-reactor system. In the first reactor, GVL undergoes decarboxylation over SiO<sub>2</sub>/Al<sub>2</sub>O<sub>3</sub> to form butene isomers and CO<sub>2</sub>. In the second reactor, butenes are oligomerized to a mixture of C<sub>8</sub>, C<sub>12</sub>, and C<sub>16</sub> alkenes over a solid acid catalyst (Amberlyst-70).<sup>37</sup> This mixture is then hydrogenated to produce a branched alkane product for inclusion in aviation fuel blends.

Two options were explored for lignin conversion: catalytic fast pyrolysis (CFP) and combustion. During CFP, lignin is fed into a fluidized bed reactor that contains a ZSM5 catalyst. In this manner, aromatics are produced including benzene, toluene, and xylenes. While CFP is able to produce aromatics in high yields from wood,<sup>38</sup> low aromatic yields are obtained during CFP of lignin residues recovered from levulinic acid production. Given the limited yields of lignin pyrolysis, process economic models reported here are focused exclusively on hydrolysis-based jet fuel production. In this strategy, as in cellulosic ethanol processes, the most likely application for lignin and humic residues is combustion for the production of heat and/or power.<sup>39</sup>

## 3 Review of central technologies in aviation fuel production

### 3.1 Biomass pretreatment

Hemicellulose, for most hardwoods and agricultural residues, is composed of xylans with side chains of (methylated) glucuronic acid, acetate, and/or arabinose.<sup>40,41</sup> It is readily hydrolyzed in hot water or dilute acids to produce xylooligomers, xylose monomers, and acetic acid. Depending on pretreatment severity, side reactions—such as dehydration or condensation to form humins—consume xylose and xylose oligomers, resulting in poor selectivity and product losses (Fig. 2).<sup>42–45</sup> Formic acid can additionally be produced during pretreatment *via* degradation pathways.

Pretreatment approaches were selected to maximize recovery of pentose sugars from hemicellulose while leaving cellulose intact for subsequent processing.<sup>46</sup> Further, compatibility with downstream processes and minimal consumption of external

resources are crucial to large scale viability. We considered two pretreatment methods: hot water extraction (autohydrolysis) and dilute acid hydrolysis. Within dilute acid hydrolysis, we have explored the use of both mineral and organic acids. Technologies were compared in terms of sugar recovery, downstream compatibility, and cost effectiveness.<sup>32</sup> Optimal sugar recoveries obtained by each pretreatment technology are summarized in Table 1.

Hot water extraction is simple, permits efficient recovery of xylooligomers, has minimal demand for additional raw materials, and requires no additional separations or catalyst recovery. Hot water extraction therefore offers low raw material costs and excellent process compatibility. Representative hot water extractions were carried out from 453–493 K using 10% hardwood loadings in an autoclave reactor (*e.g.*, Parr Instruments). Maximal hemicellulose recovery (81.6%) was achieved at 473 K after 11.2 minutes. At these conditions, 86.4% of the recovered sugars are xylooligomers and 13.4% are xylose monomers. Despite the high yield of pentoses, oligomer-rich products may hinder downstream processing. For example, hydrogenation to produce xylitol is ineffective unless oligomers are first hydrolyzed to xylose monomers.<sup>11</sup> Further, xylooligomers, particularly those with high degrees of polymerization (DP), precipitate during storage and transportation.<sup>47,48</sup> If processing delays are anticipated, it may be advantageous to hydrolyze oligomeric sugars during pretreatment to improve stability, and this is readily achieved in acidic solutions.

To target production of monomeric sugars, dilute acids may be integrated directly into pretreatment, and both organic (oxalic) and mineral (H<sub>2</sub>SO<sub>4</sub>) acids are viable options. By soaking ground red maple in 0.5 wt% H<sub>2</sub>SO<sub>4</sub> prior to pretreatment, 84.4% of feed hemicellulose was recovered in an autoclave reactor during a 27.5 minute pretreatment at 433 K with xylose monomers comprising 78.8% of the sugar distribution. Though effective in oligomer hydrolysis, care must be taken using H<sub>2</sub>SO<sub>4</sub> during pretreatment as it can inhibit or poison downstream catalytic processes, particularly those employing noble metals.<sup>49–51</sup> Organic acids, such as oxalic acid, have minimal negative impact on noble metals and can be used as an alternative to mineral acids. We observed that sugar yields obtained during oxalic acid pretreatment are comparable to those achieved using dilute H<sub>2</sub>SO<sub>4</sub> pretreatment. By treating red maple

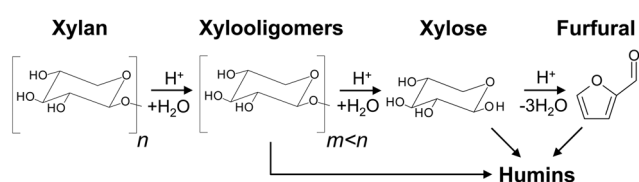


Fig. 2 Chemical reactions involved in the acid catalyzed hydrolysis of xylan and dehydration of xylose.

Table 1 Comparison of optimal sugar yields observed during autohydrolysis and dilute acid pretreatments of red maple in an autoclave reactor. Adapted from Zhang, ref. 32

Optimal pretreatment conditions	Product yields (wt%)			
	Total xylose	Monomer	Oligomers	Furfural
Autohydrolysis, 473 K, 11.2 min	81.6	13.4	68.2	3.7
0.5% Sulfuric acid 433 K, 27.5 min	84.4	78.8	5.6	5.1
0.5% Oxalic acid 433 K, 27.5 min	87.5	73.9	13.6	4.1

with 0.5 wt% oxalic acid prior to 27.5 minute hydrothermal processing at 433 K, we extracted 88% of the feed hemicellulose, with 73.9% of the carbohydrate recovered as xylose monomers and 26.1% recovered as xylooligomers. Clearly, oxalic acid is a higher cost catalyst; however, its application may be appropriate in processes that deliver high-value products and employ sulfur- or chlorine-sensitive catalysts. As an example, oxalic acid pretreatments are well-suited to production of xylitol, which requires oligomer hydrolysis, employs a noble metal hydrogenation catalyst, and is inhibited by residual chlorides and sulfates. In addition, use of oxalic acid would reduce the requirements on material of construction for the pretreatment reactor compared to using mineral acids containing more corrosive sulfates or chlorides.

Yields reported in Table 1 are given for laboratory scale autoclave reactors at roughly 10 wt% solids loadings; however, each technology was straightforward to implement in a 4 L steam gun using solid loadings as high as 50 wt%. As such, all pretreatment technologies are relatively easy to scale and can deliver efficient hemicellulose recovery in pilot or commercial settings. In the integrated process described in this article, all biomass fractions recovered from pretreatment were directly used as inputs to downstream reactors targeting alkane fuel production, and the nature of the downstream processes influenced the choice of pretreatment strategy. In the approach proposed here, hemicellulose sugars are dehydrated in the presence of HCl to produce furfural. The biphasic system employed in that step is equally effective for converting xylooligomers as it is for model xylose feedstocks, suggesting that there is no benefit to fully hydrolyzing hemicellulose during pretreatment when targeting furfural production. Solid residuals recovered from pretreatment contain cellulose and lignin since neither is hydrolyzed in hot water. Cellulose is subsequently converted to levulinic acid *via* H<sub>2</sub>SO<sub>4</sub> hydrolysis, and lignin is dried, mixed with humic residues from downstream processes, and used as a boiler feed.

### 3.2 Hemicellulose processing

Several strategies for hemicellulose upgrading were considered in this project. The two most promising were hydrodeoxygenation (HDO) of xylose or xylitol to form monofunctional intermediates and xylose dehydration to form furfural.<sup>52,53</sup> HDO research elucidated the mechanism of polyol deoxygenation over bifunctional catalysts<sup>54</sup> and enabled the design of more efficient metal-acid catalysts for the production of gasoline-appropriate oxygenates *via* hydrogenolysis.<sup>10,11</sup> However, furfural production (Fig. 3) is the preferred option when targeting jet fuels because furfural can be converted into jet fuel range alkanes in high yields.<sup>55–58</sup> HDO products are predominately mixed heterocyclic oxygenates that offer good octane numbers and are well-suited to gasoline blending; unfortunately, mixed heterocyclic species are difficult to transform into jet fuel-appropriate hydrocarbons. Furfural, on the other hand, has an existing chemical market and can be prepared, along with acetic and formic acid, in high yields using biphasic reactors. Several options exist for the conversion of

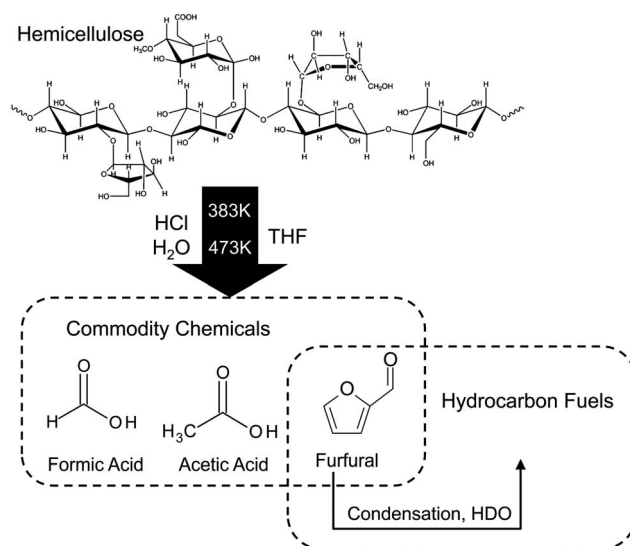


Fig. 3 Overview of commodity chemical and transportation fuel production from xylans.

furfural into jet fuel range alkanes.<sup>55–58</sup> Furfural can be hydrogenated to 2-methyl furan by commercial processes.<sup>58</sup> Corma and co-workers have shown that 2-methyl furfural can then be trimerized under acidic conditions.<sup>59</sup> This trimerized molecule can produce diesel range hydrocarbons upon hydrodeoxygenation. Alternatively, both Zhang and Corma groups have shown that the furfural can also be upgraded to diesel fuel range components using hydroalkylation-alkylation (HAA) process followed hydrodeoxygenation.<sup>55,60</sup> In this approach, 2-methyl furan derived from furfural is hydroalkylated with aldehydes and ketones such as furfural or acetone, to increase the carbon backbone of precursor molecules. These precursor molecules can be then hydrodeoxygenated to form diesel fuel range hydrocarbons. In this project, we have chosen to work on another alternative process that involves aldol condensation of furfural with acetone followed by hydrodeoxygenation.<sup>30,56,57,61</sup>

**3.2.1 Furfural production.** Hemicellulose was upgraded *via* acid-catalyzed hydrolysis and dehydration to produce furfural, acetic acid, and formic acid in a continuous biphasic reactor as shown in Fig. 4.<sup>33</sup> Aqueous hemicellulose oligomers were provided by hot water extraction as described in the above Biomass Pretreatment section. Furfural is prepared *via* sequential dehydration of pentose sugars, which are the dominant products in hardwood hemicellulose hydrolyzates. Dehydration conditions also enable side reactions to form degradation products, and the primary challenge in furfural production is maintaining good selectivity at high sugar loadings,<sup>33,62</sup> a concern which was addressed here through the use of biphasic flow reactors. Prior to introduction into the reactor, pretreatment hydrolyzates were mixed with HCl to a concentration of 0.44 M and saturated with NaCl to improve phase separation in the biphasic scheme. THF was introduced as a co-feed to create an organic extracting phase and improve furfural selectivity.

Optimal furfural yields were obtained with a plug flow reactor having two different heated zones. The initial,

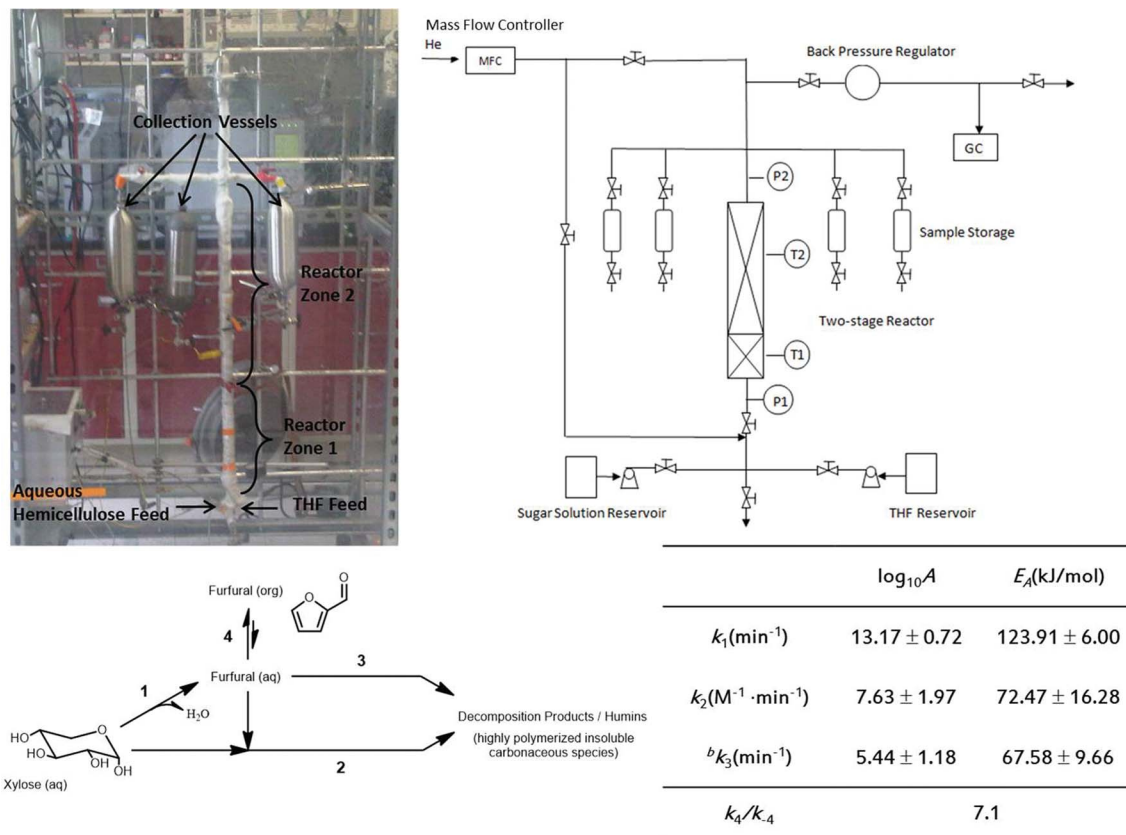


Fig. 4 Reactor schematic, actual reactor and lumped kinetic model for continuous production of furfural in a biphasic reactor. Adapted from ref. 33 and 62.

low-temperature zone facilitates hydrolysis of xylans to create pentose monomers and acetic and formic acids. This zone must achieve oligomer hydrolysis but should be operated at sufficiently low temperatures to avoid dehydration and degradation of monomeric sugars. Fig. 4 also summarizes the kinetic model developed to describe production of furfural *via* xylose dehydration.<sup>62</sup> We have observed that step 1 (xylose dehydration to produce furfural) has a higher apparent activation energy than steps 2 and 3, which lead to the formation of undesired humins. Thus xylose dehydration, occurring in zone 2, should be carried out at as high a temperature as practical to improve furfural selectivity.

Extensive variation in xylose conversion, furfural selectivity, and furfural yields were observed with changes in reaction parameters including liquid hourly space velocity (LHSV), temperature, xylose concentration, and acid concentration.<sup>33,34</sup> Maximal yields can only be achieved by balancing the kinetics of xylose dehydration with those of degradation reactions. Poor yields at low space velocities are associated with increased humin formation, whereas low yields at high space velocities are associated with kinetic limitations of xylose dehydration at short residence times. Though optimal residence times will be dictated by the exact operating conditions, high furfural yields are generally expected at low to moderate space velocities. Under these conditions, inevitable humin formation causes a slight loss in selectivity, but this is balanced by higher xylose

conversion to permit single-pass furfural carbon yields in excess of 90%.<sup>33</sup>

Furfural selectivity is reduced at elevated xylose concentrations, which is likely attributed to more prevalent degradation in increasingly concentrated aqueous phases.<sup>33,56,62–64</sup> Higher HCl concentrations are required when processing hot water extracts as compared to xylose solutions, an effect which arises from the additional requirement of oligomer hydrolysis prior to xylose dehydration. Though optimal furfural selectivities have been previously reported (with model xylose solutions) using 0.22 M HCl,<sup>64</sup> concentrations of 0.44 M were necessary in this study when processing hot water extracts. Higher acid loadings (0.6 M) lead to increased humin formation and reduced furfural selectivity.

Furfural yields were insensitive to zone 1 temperature when variations were studied at a fixed zone 2 temperature (473 K). Furfural carbon yields varied between 85 and 90% over a range of zone 1 temperatures (343–413 K) with a slight maximum observed at 383 K. The general requirements of the first reactor are that temperature and acidity must be sufficient to initiate oligomer hydrolysis but not so high as to contribute to degradation. Zone 2 temperature had a more profound effect on furfural yields. While high furfural carbon selectivities (>90%) were observed over a range of temperatures (433–493 K), high xylose conversions were only achieved (LHSV of  $1.4 \text{ h}^{-1}$ ) at temperatures of 473 K and above, an outcome which is

attributed to the fact that xylose dehydration does not occur at appreciable rates below 473 K.<sup>33</sup>

Table 2 summarizes compositions of representative feeds to and products from the first and second stages of the above furfural production strategy. The overall furfural carbon yield obtained in the experiment detailed in Table 1 was in excess of 90%. When processing hot water extracts, significant quantities of acetic and formic acids and trace quantities of HMF form alongside hydrolysis and dehydration products. HMF forms through dehydration of trace hexose sugars, while the organic acids form either through hydrolysis of acetyl side chains in hemicellulose or degradation pathways. The majority of reaction products are recovered in the THF extracting phase while unconverted sugars—along with minor quantities of reaction products—are retained in the aqueous phase.

At this stage, it is appropriate to consider the outputs of furfural production (from hemicellulose hydrolyzates) and the downstream options they enable. Reclamation of formic acids does not presently appear cost effective; however, acetic acids are recovered from THF through a distillation sequence and could be sold or optionally utilized within integrated bio-refineries.<sup>33</sup> For example, ketonization of acetic acid would enable production of acetone and could be achieved with high yields over CeZrO<sub>x</sub>.<sup>65–67</sup> Furfural is converted to mixed alkanes *via* aldol condensation and subsequent hydrodeoxygenation.

**3.2.2 Alkane production from furfural.** Furfural can be converted into heavy alkanes through the three basic steps outlined in Fig. 5. First, furfural is condensed with acetone in basic media to produce conjugated C<sub>13</sub> compounds, referred to herein as furfural–acetone–furfural (FAF). In a second stage,

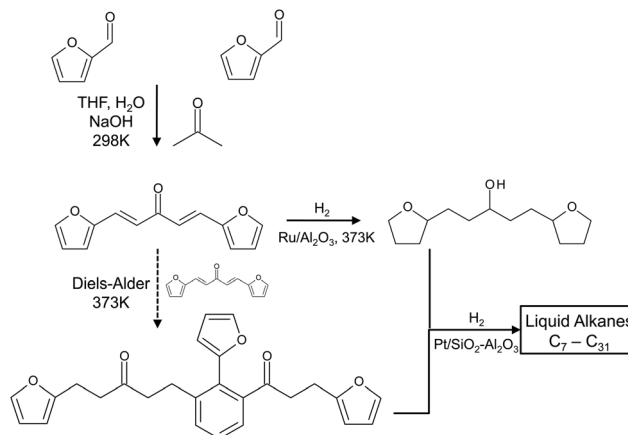


Fig. 5 Overview of chemistry involved in the production of linear and branched alkanes from furfural and acetone.

condensation products are hydrogenated over a supported noble metal (*e.g.*, Ru/Al<sub>2</sub>O<sub>3</sub>) at low temperatures to improve their thermal stability. During the hydrogenation step, conjugated intermediates condense *via* Diels–Alder reaction to form heavy (<C<sub>31</sub>) oxygenates.<sup>57</sup> In a final stage, products of the low-temperature hydrogenation step are processed, along with a hydrogen co-feed, over bifunctional catalysts to eliminate the remaining oxygen and isomerize a portion of the product to form a mixture of linear and branched alkanes with carbon numbers up to C<sub>31</sub>.

**Aldol condensation.** Furfural condensation was carried out in biphasic batch reactors using a THF organic phase and an aqueous phase containing a sodium hydroxide catalyst and various concentrations of NaCl. Furfural and acetone were introduced to the reactor in a 2 : 1 ratio in THF and subsequently mixed with the basic aqueous phase to initiate condensation. Complete furfural conversions were observed at all conditions tested; however, selectivity to the FAF product varies significantly with operating conditions. Condensation selectivity was weakly dependent upon NaCl concentration, and salt addition was eliminated in final protocols to reduce raw material and separations expenses. FAF selectivity was improved by operating at higher NaOH concentrations, higher organic : aqueous ratios, lower temperatures, and longer residence times. FAF yields of 96.2 carbon% have been demonstrated in a 200 ml batch reactor by operating with 36.8 wt% furfural in THF at an organic to aqueous mass ratio of 5.1 : 1 and a NaOH to furfural ratio of 0.37 : 1.<sup>34</sup> These conditions allow nearly quantitative production of FAF using relatively high furfural feed concentrations, small aqueous phase volumes, and reduced NaOH quantities compared to prior studies.<sup>68</sup> A slight loss of furfural selectivity is observed at high NaOH concentrations. Under these conditions, Michael additions are favored and couple furfural–acetone (FA) and furfural–acetone–furfural (FAF) adducts to form oligomeric species. However, Michael addition products can be co-processed alongside FAF in subsequent hydrogenation and hydrodeoxygenation steps to allow ultimate incorporation into fuel products.<sup>57</sup>

**Table 2** Composition of the hemicellulose solution obtained from hot water extraction of mixed northern hardwood chips and products obtained using the biphasic, two-temperature zone plug flow reactor. The first temperature zone was comprised of a 25.4 cm × 1.27 cm stainless steel tube packed with 4 mm glass beads, and the second temperature zone was comprised of a 22.9 cm × 1.27 cm stainless steel tube packed with quartz tubes (1 mm ID, 2 mm OD, 2 mm L). Reaction conditions:  $T_1 = 383$  K,  $T_2 = 473$  K, LHSV = 1.44 h<sup>-1</sup>,  $V_{org}/V_{aq} = 2.0$  and  $[H^+] = 0.44$  M. Reproduced from ref. 33

	Feed concentration (mmol L <sup>-1</sup> )		Product concentration (mmol L <sup>-1</sup> )	
	Before hydrolysis	After hydrolysis <sup>a</sup>	Aqueous phase	Organic phase
Xylose	171.1	713	20.3	—
Glucose	20.7	62.6	10.0	—
Arabinose	38.5	38.5	—	—
Acetic acid	70.4	307.4	69.3	296.4
Lactic acid	2.1	7.1	—	—
Formic acid	22.6	25.2	106.7	132.3
Furfural	9.8	35.6	18.4	319.8
HMF	—	—	2.6	20.4
TOC (ppm)	99992.0	—	41981.6	—
Identified carbon	16727.2	59692.8	6044.6	32986.5

<sup>a</sup> Hemicellulose hydrolyzates were obtained by treating hot water extracts with 0.44 M HCl at 383 K and are included here to indicate expected compositions of the aqueous phase effluent from zone 1, which was not typically analyzed.

**Low Temperature Hydrogenation.** FAF products were hydrogenated in THF over Ru/Al<sub>2</sub>O<sub>3</sub> at low temperatures in a batch reactor (353–413 K). Over Ru sites, the C=C and C=O groups in aldol products are hydrogenated to form stabilized C<sub>13</sub> oxygenates that may be subsequently converted to alkanes using bifunctional hydrodeoxygenation catalysts. In parallel, we observe two additional classes of chemistry during low temperature hydrogenation, both of which will be considered briefly here since they affect product selectivities. For the interested reader, analysis of the mechanisms and pathways is detailed in prior studies.<sup>57</sup> The first parallel pathway is non-catalytic coupling of aldol adducts and partially hydrogenated furanic intermediates *via* cycloaddition to create heavy oligomers.<sup>69</sup> The second competing pathway is cracking of aldol adducts or cycloaddition products, which occurs over Ru/Al<sub>2</sub>O<sub>3</sub> to yield light hydrocarbons.<sup>57</sup> Each pathway occurs to some extent at all conditions tested, and selectivities can be tailored toward light hydrocarbons (<C<sub>13</sub>), tridecane (C<sub>13</sub>), or heavy hydrocarbons (>C<sub>13</sub>) as desired. For example, high temperatures (413 K) and hydrogen pressures (8.27 MPa) favor cracking and increase selectivity to light products such that they can account for nearly 30% of the total carbon yield. Lower temperatures allow higher selectivity to C<sub>13</sub> and heavier hydrocarbons, and high FAF feed concentrations and hydrogen pressures encourage oligomer production. For example, when operating with a feed comprised of 10 wt% condensation products (primarily FAF in THF), 53% carbon selectivity to C<sub>13</sub> is observed at 8.3 MPa. At 5.5 MPa, C<sub>13</sub> carbon selectivity improves to 75% and is accompanied by a decrease in oligomer carbon selectivity from 29% to 18% along with a 50% reduction in cracking. Selectivity is shifted to heavy products (up to 49 carbon%) by increasing the feed concentration to 30 wt% FAF and operating at 8.3 MPa.

**Hydrodeoxygenation.** The final step in producing alkane fuels from furfural is hydrodeoxygenation. In this stage, products of low temperature hydrogenation—including C<sub>13</sub> hydrocarbons, light cracking products, and heavy hydrocycloaddition products—are processed with a H<sub>2</sub> co-feed over a bifunctional (metal–acid) catalyst to facilitate sequential dehydration and hydrogenation reactions that yield saturated alkanes.<sup>30,70</sup> In this program, Pt–SiO<sub>2</sub>/Al<sub>2</sub>O<sub>3</sub> was employed at 573 K and 8.3 MPa of H<sub>2</sub> for HDO, and this approach was selective for production of paraffinic, branched, and cyclic alkanes. Formation of light hydrocarbons (C<sub>1</sub>–C<sub>6</sub>), CO, and CO<sub>2</sub> did occur through cracking and decarbonylation; however, total selectivities of gas phase carbon were generally maintained below 20 carbon%.

Given the relatively high selectivity achieved during HDO, the product alkane distribution depends most strongly on the composition of the HDO feed. Fig. 6 summarizes NOISE<sup>71</sup> analysis of representative alkane blends obtained through HDO of two different feed mixtures. Feeds rich in hydrogenated FAF (Fig. 6, blue columns) primarily resulted in formation of C<sub>12</sub> and C<sub>13</sub> straight chain alkanes, while feeds rich in cycloaddition products (Fig. 6, red columns) formed a broad distribution of liquid alkane products ranging from C<sub>8</sub> to C<sub>27</sub> and containing a mixture of linear, branched, and cyclic alkanes. The

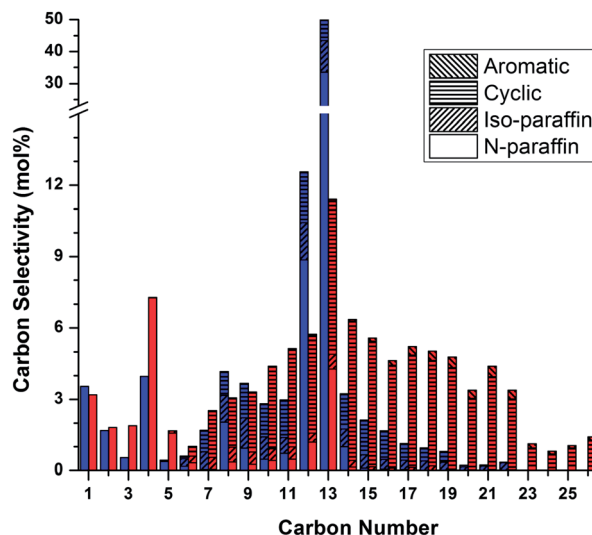


Fig. 6 Molar carbon selectivities for different renewable petroleum refinery feedstocks derived from aqueous xylose feedstocks. These products were obtained by low-temperature hydrogenation and hydrodeoxygenation of condensed furfural–acetone mixtures. Feed compositions: blue (74.7% hydrogenated dimer; 7.21% lights; 18.1% heavies) and red (1.32% hydrogenated dimer; 7.65% lights; 91.0% heavies). Hydrodeoxygenation reactions were conducted at 573 K and 8.27 MPa over 2.5 g 4% Pt/SiO<sub>2</sub>–Al<sub>2</sub>O<sub>3</sub> catalyst. Figure adapted from ref. 57.

hydrocarbon product distribution obtained through this process has similar properties to light and heavy cycle oils and thus provides a renewable alternative for the production of refinery feedstocks.<sup>57</sup>

### 3.3 Cellulose processing

**3.3.1 Levulinic acid production.** Cellulose is the dominant carbohydrate in lignocellulosic biomass, comprising roughly 42 wt% of the representative hardwood samples considered in this research program.<sup>32,46</sup> In acidic media, cellulose will hydrolyze, forming glucose, which subsequently dehydrates to yield 5-HMF. HMF subsequently can condense with other HMF monomers or glucose, leading to humin formation and reducing product yields. Ultimately, in acidic aqueous solutions, HMF will hydrate to form levulinic acid (LA) and formic acid (FA). A summary of the various acid-catalyzed steps and products formed is given in Fig. 7.

Pretreated cellulose–lignin residuals were hydrolyzed in aqueous mineral acids (HCl or H<sub>2</sub>SO<sub>4</sub>) from 453 to 493 K over a range of residence times in a batch reactor. The highest levulinic acid yields were obtained through sulfuric acid hydrolysis (1.5 wt% H<sub>2</sub>SO<sub>4</sub>) of pretreated cellulose (10 wt % solids loading) at 473 K. At these conditions, a 45 minute residence time delivered 75.5% of the maximum theoretical molar yield of LA. Comparable yields were observed when operating at 50 wt% solid loading in a 4 L steam gun; however, operating conditions were modified slightly to account for the higher solids loading. Specifically, the steam gun required longer residence times (60 minutes) to achieve complete cellulose conversion at 473 K. The steam gun was employed for supplying project

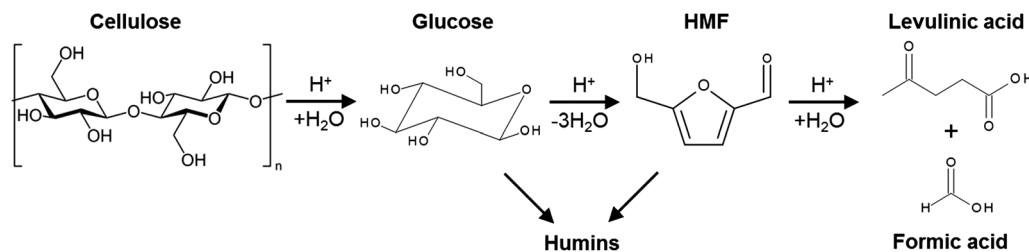


Fig. 7 Chemical reactions in the acid catalyzed hydrolysis of cellulose leading to the formation of levulinic and formic acids.

Table 3 Representative composition of cellulose hydrolyzates obtained by treatment with 1.5 wt% H<sub>2</sub>SO<sub>4</sub> at 473 K for 60 minutes in a 4 L steam gun

	Concentration	
	g L <sup>-1</sup>	mol L <sup>-1</sup>
Sulfuric acid	15.2	0.155
Levulinic acid	53.8	0.460
Formic acid	10.1	0.220
5-HMF	1.85	0.015
Glucose	13.3	0.075
Xylose	1.00	0.007

collaborators with unrefined LA feedstocks, and a representative composition of these hydrolyzates is summarized in Table 3. Viable LA yields were observed only by using HCl and H<sub>2</sub>SO<sub>4</sub> as catalysts. Total LA yields were slightly higher (by 10%) when employing H<sub>2</sub>SO<sub>4</sub> as compared to HCl, indicating that it is slightly more selective. However, HCl appears more intrinsically active such that higher acid loadings or longer residence times are required when using H<sub>2</sub>SO<sub>4</sub>. For the process described here, H<sub>2</sub>SO<sub>4</sub> was preferred for its lower cost, reduced corrosiveness, and improved LA selectivity. Further, residual sulfates are more easily separable and had less impact upon downstream LA processing than residual chlorides.

Fig. 7 indicates that LA and FA should be produced in equal concentrations; however, hydrolyzates recovered from the steam gun had FA concentrations that were roughly half of the LA concentration (Table 3). This is a consequence of the different volatilities of LA (boiling point 519 K) and FA (boiling point 374 K). As the steam gun is an open system, relatively volatile FA is lost to the vapor phase, while LA is retained in the liquid phase. In contrast, when hydrolysis was carried out in an autoclave reactor (Parr), hydrolyzate concentrations of LA (0.460 mol L<sup>-1</sup>) and FA (0.462 mol L<sup>-1</sup>) were nearly equal. This supports a loss of FA to the vapor phase in the steam gun and indicates that this FA recovery should be optimized prior to their scale up.

**3.3.2 GVL production.** Levulinic acid can be used for production of specialty or commodity chemicals, or it can be upgraded to jet fuel through intermediate formation of  $\gamma$ -valerolactone, a strategy which is summarized in Fig. 8. GVL is prepared by hydrogenation of LA, and numerous studies have reported the suitability of both homogeneous<sup>17,20</sup> and

heterogeneous<sup>18,72,73</sup> Ru-based catalysts for this reaction. Further, FA dehydrogenation over Ru,<sup>17,19,74–76</sup> Pd,<sup>12,77</sup> or Au<sup>78</sup> can supply *in situ* H<sub>2</sub> for LA reduction.<sup>16,17,20,79</sup> The majority of prior LA hydrogenation studies have been carried out using model aqueous LA feedstocks, and limited consideration has been given to the implications of acid or biomass residuals on catalytic hydrogenation. We have observed that typical heterogeneous catalysts used in reducing LA are profoundly affected by such impurities and have determined that GVL production strategies will depend strongly upon the extent to which raw cellulose hydrolyzates are purified prior to hydrogenation.

Residual H<sub>2</sub>SO<sub>4</sub> critically impairs the activity of Ru/C during LA reduction,<sup>49</sup> and its management is central to achieving good hydrogenation rates. A straightforward option for H<sub>2</sub>SO<sub>4</sub> removal is precipitation of gypsum from raw LA hydrolyzates *via* addition of Ca(OH)<sub>2</sub>, and neutralization does enable the use of Ru/C in model systems; however, with lignocellulose-derived LA feedstocks, it was necessary to carry out hydrogenations under alkaline conditions (pH = 11) to achieve high GVL yields. Though this effect was not characterized in detail, we believe that alkalinity facilitates precipitation of biomass-derived impurities, such as acid-soluble lignin, which inhibit catalytic activity if retained in solution. It is important to note that, under these conditions, levulinic acid and formic acid exist respectively as calcium levulinate and calcium formate, though both are water soluble and are thus not removed along with gypsum during filtration. Though superficially simple, neutralization presented a number of processing challenges that may hinder the scalability of the approach. For example, the requirement of highly alkaline conditions increases Ca(OH)<sub>2</sub> consumption, adding to raw material costs. Further, gypsum retains a significant portion of the aqueous hydrolyzate during filtration and requires extensive washing to recover more than 90% of the levulinate and formate salts. Repeated washings result in low filtrate concentrations such that a portion of the water needs to be evaporated prior to hydrogenation to concentrate the salts and reduce reactor sizes.

As an alternative, bimetallic catalysts (*e.g.*, RuRe/C) permit direct hydrogenation of LA in the presence of H<sub>2</sub>SO<sub>4</sub>, eliminating the need for acid neutralization or inter-stage separations.<sup>49,74</sup> Operating at 423 K and 35 bar H<sub>2</sub> in 0.5 M H<sub>2</sub>SO<sub>4</sub>, comparably high selectivity and GVL carbon yields (>99%) were observed over both Ru/C and RuRe/C; however, the bimetallic system offered improved stability, with the addition of Re preventing catalyst deactivation. An advantage of this approach is

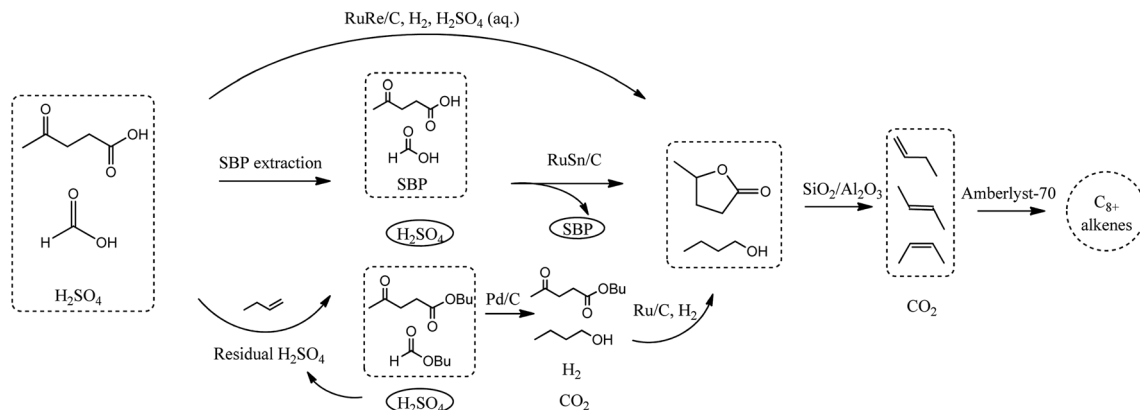


Fig. 8 Summary of catalytic pathways to convert levulinic and formic acid into  $C_{8+}$  alkenes via GVL and butenes. The various schemes for sulfuric acid management outlined in the text are illustrated conceptually here. In the interest of clarity, this figure does not include the neutralization pathway.

that GVL is more hydrophobic than LA and can therefore be extracted using low-boiling solvents, such as ethyl or butyl acetate, establishing relatively facile downstream recovery of both GVL and the extracting solvent.<sup>49,80</sup> Some drawbacks of the approach are the requirement of exotic materials of construction in the hydrogenation reactor to accommodate dilute  $H_2SO_4$  at high temperatures. Further, in the presence of  $H_2SO_4$ , overall GVL production rates are low ( $0.005 \text{ mmol GVL min}^{-1} \text{ g}^{-1}$ ), necessitating potentially impractical residence times, reactor sizes, and loadings of precious metal catalysts.<sup>49</sup> Finally, this method has not been fully characterized with lignocellulose-derived LA feedstocks. It is likely that impurities present in raw hydrolyzates will inhibit LA hydrogenation over bimetallic catalysts similar to inhibition observed during neutralization studies described in the preceding paragraph.

Another strategy for acid management and GVL production was based upon esterification of levulinic and formic acids using either butene or butanol in the presence of catalytic  $H_2SO_4$  retained in cellulose hydrolyzates.<sup>12,14,81,82</sup> This step results in the formation of hydrophobic butyl esters, which separate spontaneously from the acidic aqueous phase. Butyl formate and butyl levulinate can subsequently be processed, along with a water co-feed, using a single reactor in which butyl formate is first converted to  $H_2$ ,  $CO_2$ , and butanol over a bed of Pd/C, and butyl levulinate is subsequently converted to GVL and butanol *via* hydrogenation over a second bed of Ru/C. Operating at 443 K and 35 bar of  $H_2$ , GVL carbon yields of over 95% can be achieved. This strategy is attractive because it utilizes internally produced butene as an extracting agent for LA and FA recovery. Further, the two equivalents of butanol co-produced alongside GVL during ester hydrogenation can be dehydrated over  $SiO_2/Al_2O_3$  in parallel to GVL decarboxylation (downstream) to regenerate the butene required for extraction.<sup>12</sup> Finally,  $H_2SO_4$  was recovered quantitatively in the aqueous phase such that the acid catalyst is easily reused in subsequent hydrolysis cycles. A potential constraint with this approach is that concentrated solutions of LA and FA (over 6 M) are required to establish favorable esterification equilibrium in water.<sup>12</sup> As raw hydrolyzates are available at roughly 0.5 M LA and FA, water

evaporation represents a significant energy input and may limit practical implementation.

The preferred method for LA recovery is the use of alkylphenol solvents (specifically, 2-secbutylphenol, SBP) since they efficiently partition LA from dilute  $H_2SO_4$  with minimal solvent volumes. Additionally, they have no affinity for sulfuric acid or water and permit quantitative recovery of the acidic aqueous phase for subsequent cycles of cellulose hydrolysis. Subsequently, LA is hydrogenated in the presence of SBP without intermediate distillation.<sup>36</sup> Since solvent aromaticity is critical for effective partitioning of LA, it is essential that the hydrogenation step reduce only the carbonyl group of LA as opposed to the aromatic ring in SBP. In this respect, Sn promotion of Ru facilitates the required selectivity and additionally suppresses deep-hydrogenation of GVL to form products such as pentanediol or 2-methyltetrahydrofuran (MTHF).<sup>20</sup> Further, Sn-promotion confers stability to the catalysts and eliminates the irreversible deactivation that has been observed over monometallic Ru/C.<sup>35</sup> Importantly, SBP has an exceptionally high partition coefficient for GVL—on the order of 20. Considering this alongside the exclusive selectivity of RuSn/C, GVL/SBP effluents from the hydrogenation step can be used for multiple cycles of LA extraction and hydrogenation. In this manner, GVL concentrations in the SBP extracting phase can be increased fourfold, substantially improving the energy efficiency of GVL distillation.<sup>36</sup>

**3.3.3 GVL conversion.** Once formed, GVL is processed in a two-stage catalytic strategy that converts it into liquid alkenes in a molecular weight range appropriate for inclusion in jet fuels.<sup>37</sup> The process consists of two fixed-bed catalytic reactors and two vapor-liquid separators. GVL decarboxylation to form butene and  $CO_2$  occurs in the initial reactor over  $SiO_2/Al_2O_3$  at 648 K and 35 bar with a weight hourly space velocity (WHSV) of  $0.18 \text{ h}^{-1}$ . Both butene and  $CO_2$  are subsequently fed to a second reactor where butene oligomerization occurs over Amberlyst-70 or H-ZSM-5 to form higher alkenes. The integrated system operated for more than 200 hours on stream with 75% overall carbon yield to  $C_{8+}$  alkenes. Detailed mechanistic and kinetic studies on the combined acid-catalyzed ring opening and

decarboxylation of GVL over  $\text{SiO}_2/\text{Al}_2\text{O}_3$  have revealed insights into fundamental aspects of GVL decarboxylation. Briefly, pentenoic acid isomers have been identified as key intermediates that are formed *via* ring opening of GVL and subsequent isomerization over acid sites. The compiled experimental results suggest that decarboxylation occurs *via* acyclic, carboxylic acid intermediates that have a  $\beta$ -carbenium ion.<sup>83,84</sup>

The major difficulties associated with scale-up of this technology are deactivation of  $\text{SiO}_2/\text{Al}_2\text{O}_3$  during the initial 24 hours on stream and profound water inhibition during butene oligomerization.<sup>37</sup> In the decarboxylation reactor, catalyst stability can be managed through introduction of water by maintaining GVL concentrations below 60 wt% (6 M) in the feed. As such, a water co-feed to the decarboxylation reactor is required for stable catalytic activity; however, this must be balanced with the demand for a relatively dry oligomerization feed. Specifically, over Amberlyst-70 at 17 bar and 443 K, introducing 10 mol% water into an equimolar butene/ $\text{CO}_2$  feed decreases butene conversion by 50%, while increasing to an equimolar quantity of water completely suppresses butene conversion.<sup>37</sup> In integrated strategies, water was removed from the process stream using a simple, inter-reactor phase separator that was temperature controlled between 373 K and 398 K and maintained at reactor pressure (35 bar). Under these conditions, over 98% of the water in the process stream is condensed while butene and  $\text{CO}_2$  are transferred downstream in the vapor phase.<sup>37</sup> Preliminary conditions outlined for high yields in this system scaled well to larger reactors employed for liter-scale production from lignocellulosic GVL in the SurfCat program (Table 4).

The process is sufficiently robust to accommodate lignocellulose-derived GVL prepared from LA hydrolyzates after neutralization with  $\text{Ca}(\text{OH})_2$ . To benchmark stability of the system, maple-derived GVL was fed to the reactor continuously for 200 h, and no significant loss of activity was observed. After 200 h, the feed was changed to a 6 M solution of commercial

GVL (Sigma Aldrich, >98%) in deionized water and operated continuously for another 300 h at identical conditions. Product yields and system stability were found to be independent of the GVL source. Overall carbon yields for the production of  $\text{C}_{8+}$  oligomers (from lignocellulose-derived GVL) were >78% with 99% GVL conversion and >97% butene yields in the first reactor. The composition of the olefin oligomer product derived from maple-sourced and commercial GVL is summarized in Table 4. These results indicate that the performance of maple-derived GVL is comparable to that observed using model compounds. To allow final blending with hemicellulose derivatives, the alkene mixture summarized in Table 4 was hydrogenated using Ru/C at 403 K and 34 bar  $\text{H}_2$ . Alkane analogs of the skeletal isomers were obtained in nearly quantitative yields.

### 3.4 Catalytic fast pyrolysis for aromatic production

Fast pyrolysis involves rapidly heating substrates to relatively high temperatures (673–873 K) under inert atmospheres. When processed in this manner, biomass rapidly depolymerizes to form pyrolysis vapors—a mixture of light hydrocarbons and oxygenates—which condense upon cooling to form a complex bio-oil.<sup>85</sup> Compared to hydrocarbon fuels, bio-oils are relatively acidic, contain a large quantity of oxygen, and have a low heating value; as such, bio-oils typically require upgrading prior to use in combustion engines. This can be achieved *in situ* through catalytic fast pyrolysis (CFP), which is carried out in a fluidized bed.<sup>38,86</sup> A modified ZSM5 catalyst is added to the fluidized bed to convert pyrolysis vapors directly into aromatics and olefins. An overview of reaction pathways involved in CFP of cellulose is illustrated in Fig. 9.

Cellulose decomposes to anhydrosugars through homogeneous dehydration reactions, which have a relatively high barrier.<sup>87</sup> This non-catalytic step competes with slow pyrolysis, which leads to formation of coke, water and  $\text{CO}_2$ . Selectivity towards anhydrosugars in fast pyrolysis is facilitated by high heating rates, which necessitates small biomass particles.<sup>88</sup> Anhydrosugars dehydrate further during fast pyrolysis, forming furanic compounds alongside water and  $\text{CO}_2$ . Furan formation can occur both in the gas phase and at acid sites on catalyst surfaces,<sup>89</sup> while subsequent furan conversion occurs predominantly within the catalyst pore structure. Specifically, furanic species undergo a series of acid catalyzed dehydration, oligomerization, decarboxylation, and decarbonylation reactions, ultimately yielding olefins and monocyclic aromatics through intermediate formation of a hydrocarbon pool.<sup>89–92</sup> Polycyclic aromatic species are then formed by subsequent coupling of monocyclic aromatics with oxygenated intermediates.<sup>93</sup> Intra-particle reactions leading to aromatic formation compete with parallel pathways that result in coke formation; thus, physical and chemical properties of acidic solids are critical to maximizing aromatic and olefin yields during fast pyrolysis.

CFP research in this program was carried out using a variety of reactor configurations. Pyroprobe studies were used for fundamental investigations and catalyst optimization, while fluidized beds were used to explore lignin pyrolysis and technology scaling. The details of both are discussed in prior

**Table 4** Summary of the performance of the two-reactor GVL decarboxylation system employed for the production of alkene oligomers from commercial and lignocellulose-derived GVL. For both studies, the first reactor contained  $\text{SiO}_2/\text{Al}_2\text{O}_3$  and operated at 648 K and 35 bar with a GVL WHSV of  $0.18 \text{ h}^{-1}$ . The second reactor contained Amberlyst-70 and operated at 443 K and 35 bar with a GVL WHSV of  $0.15 \text{ h}^{-1}$

		Maple wood derived GVL	Commercial GVL
Decarboxylation reactor ( $\text{SiO}_2\text{-Al}_2\text{O}_3$ )	GVL conversion (%)	98	99
	Butene molar yield (%)	97	98
Oligomerization reactor (Amberlyst-70)	Butene conversion (%)	95	94
Final oligomers composition (%)	$\text{C}_{8-}$	9	13
	$\text{C}_8$	21	24
	$\text{C}_{12}$	22	24
	$\text{C}_{16}$	23	22
	$\text{C}_{20}$	14	12
	$\text{C}_{20+}$	10	6

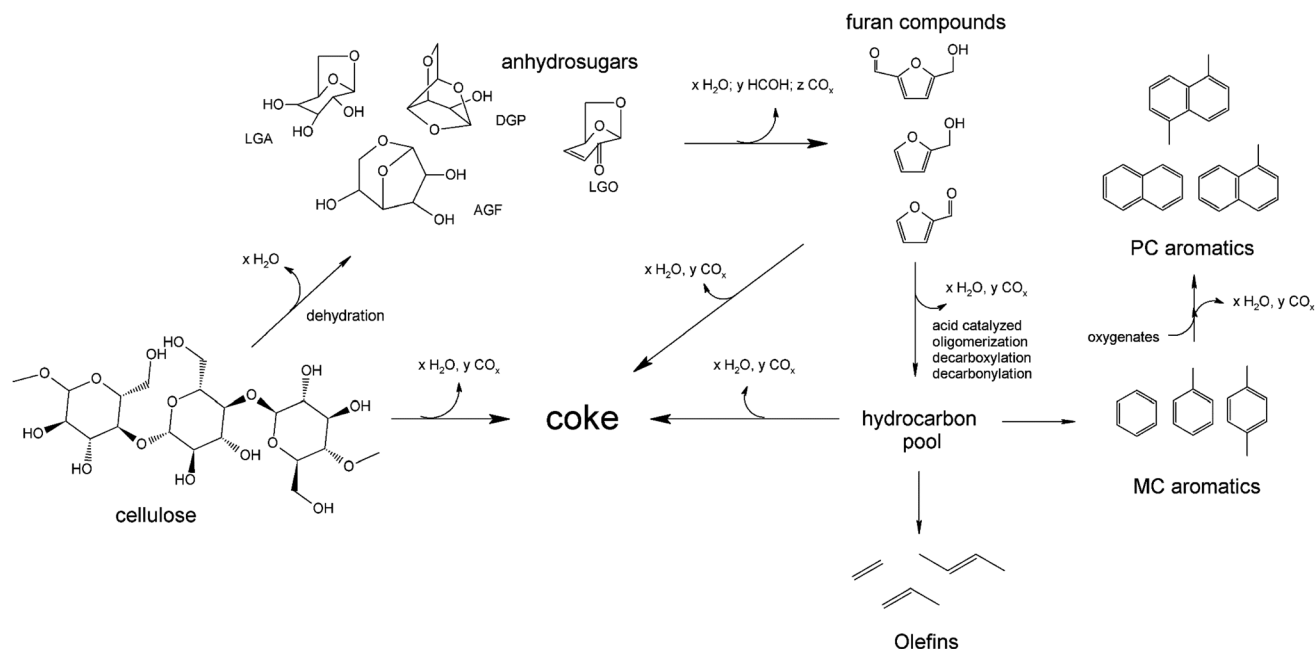


Fig. 9 Landscape of reactions occurring during the catalytic fast pyrolysis of cellulose. Reproduced from ref. 38.

publications.<sup>38,89,94,95</sup> Aromatic yields during CFP are determined by both the pyrolysis feedstock and the characteristics of the catalysts employed.<sup>96</sup> ZSM-5 is the preferred base zeolite for CFP.<sup>95–99</sup>

Zeolite micropores impart shape selectivity during pyrolysis of glucose in pyroprobe reactors.<sup>95</sup> Over a series of small pore (ZK-5, SAPO-34), medium pore (Ferrierite, ZSM-23, MCM-22, SSZ-20, ZSM-11, ZSM-5, IM-5, TNU-9), and large pore zeolites (SSZ-55, Beta zeolite, Y zeolite), aromatic yields are a function of

zeolite pore size (Fig. 10). Small pore zeolites ( $<5 \text{ \AA}$ ) produced negligible amounts of aromatics and oxygenates, favoring instead the formation of  $\text{CO}$ ,  $\text{CO}_2$ , and coke. Medium pore zeolites ( $5.2\text{--}5.9 \text{ \AA}$ ) gave the highest aromatic yields (10–35% on carbon basis), while large pore zeolites coked heavily at the expense of selectivity to aromatics and small oxygenates. Comparison of kinetic diameters of the products and reactants with zeolite pore dimensions suggests that the majority of species can diffuse into medium and large pore zeolites.

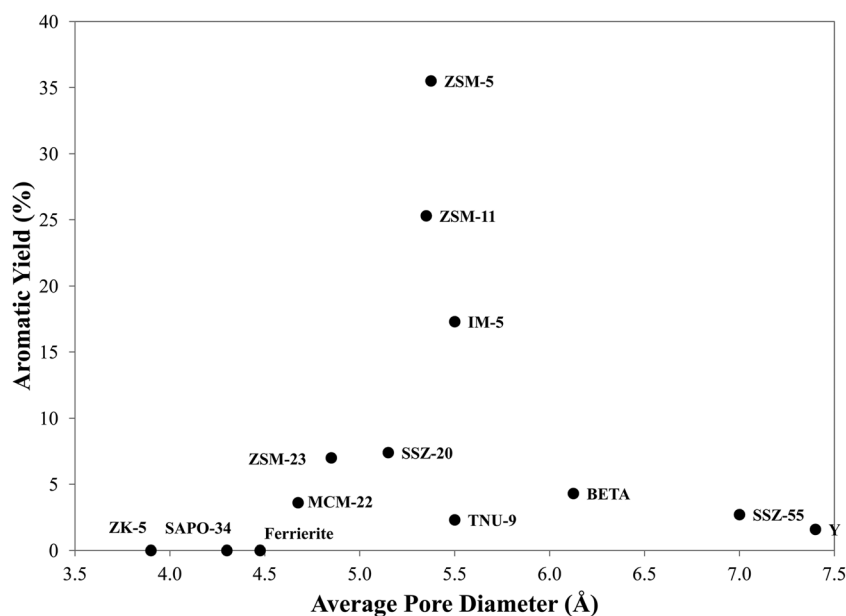


Fig. 10 Aromatic yields as a function of average pore diameter for different zeolites during catalytic fast pyrolysis of glucose in a pyroprobe reactor. Reaction conditions: catalyst-to-feed weight ratio = 19, nominal heating rate  $1273 \text{ K s}^{-1}$ , reaction time 240 s. This figure has been reprinted from Jae, *et al.* (ref. 95) with permission from the publisher.

However, internal diffusion is constrained in smaller pore zeolites, indicating that reactions occur on external acid sites where polycyclic aromatics appear to form readily. ZSM-5 was shown to offer an appropriate combination of pore size and cavity dimensions for the production of aromatics during CFP.<sup>89,96</sup>

Subsequently, we explored post-synthetic zeolite modifications in an effort to improve aromatic yields. Low yields observed over small-pore zeolites suggest that external acid sites are non-selective toward aromatics and instead favor coke formation. To decrease external surface acidity, ZSM-5 samples were treated with tartaric acid. As tartaric acid is too large to diffuse through zeolite micropores, it selectively leaches Al from external surface sites.<sup>100</sup> To facilitate diffusion of pyrolysis intermediates in catalyst particles, mesoporosity was introduced to selected ZSM-5 samples using the surfactant-mediated method reported by Ryoo, *et al.*<sup>101</sup> Pyroprobe studies of various feedstocks (furan, glucose, maple wood, *etc.*) demonstrated that neither removal of external surface acid sites nor formation of hierarchical mesopores improved aromatic yields,<sup>94</sup> which is consistent with prior literature.<sup>102,103</sup> However, a distinct difference in selectivity is observed when comparing mesoporous and purely microporous ZSM-5 (Fig. 11). Mesoporous samples favor production of larger alkylated monoaromatics (C<sub>9</sub> & C<sub>10</sub>), and microporous analogs form small quantities of C<sub>9+</sub> aromatics. This effect has similarly been reported during pyrolysis of propanal.<sup>104</sup> In addition, mesoporous ZSM-5 decreased selectivity toward polyaromatic species.

To date, chemical modification of spray-dried ZSM-5 has provided the most significant enhancement in aromatic yields. During CFP of pine sawdust at 823 K and a WHSV of 0.35 h<sup>-1</sup>, isomorphous substitution of Ga into the Al-ZSM-5 framework

improves aromatic carbon yields from 15 to 23%, while the combined carbon yield of aromatics and olefins increases from 29.3 to 42.7%. The activity of Ga-ZSM-5 appears to be bifunctional, with Ga facilitating decarbonylation and olefin aromatization, while Brønsted acid sites catalyze cracking, oligomerization, and aromatization.<sup>105</sup>

**3.4.1 Catalytic fast pyrolysis of lignin residues.** Lignin and humic residues are generally believed to consist of polyaromatic compounds with phenolic functionalities. Hence, lignin could potentially be used for the production of aromatics. In this project, catalytic fast pyrolysis was explored as a potential technology for converting lignin residues into value-added monomers. Lignin fast pyrolysis experiments were carried out in a 4'' fluidized bed reactor designed for continuous addition and regeneration of catalysts. Table 5 compares yields and product distributions obtained from catalytic fast pyrolysis of maple wood and lignin residues in the fluidized bed. Lignin residue was recovered after LA production *via* H<sub>2</sub>SO<sub>4</sub> hydrolysis and contains both lignin and humic residues. The data reported here reflect product yields obtained during the initial 30 minutes on stream. CFP of lignin samples produced lower yields (on a carbon basis) of aromatic hydrocarbons (2%) and a significantly higher yield of coke (70%) than that observed during analogous CFP of maple wood (15% aromatics, 32% coke).

To reveal insights into the decreased yields, the kinetics of lignin pyrolysis were studied using thermogravimetric analysis and pyroprobe GC-MS experiments.<sup>106</sup> We observed that a lumped, two-step kinetic model captures trends observed during the pyrolysis of lignin residues obtained from maple wood. The first step of lignin pyrolysis takes place over a wide

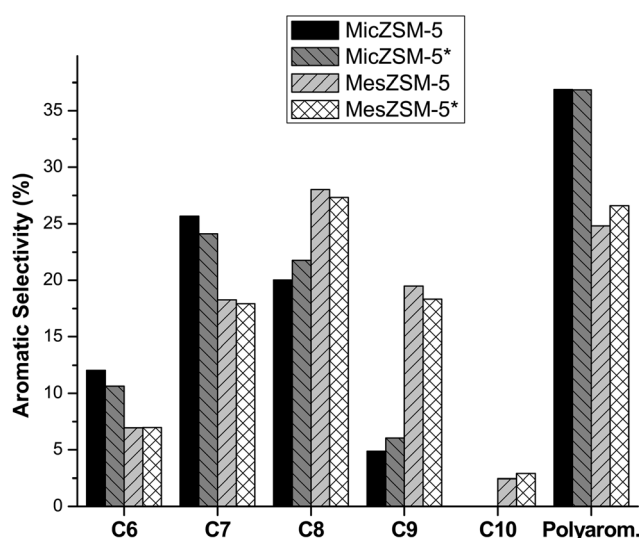


Fig. 11 Distribution of aromatic products from catalytic fast pyrolysis of maple wood over microporous ZSM-5 (MicZSM-5), tartaric acid-treated ZSM-5 (MicZSM-5\*), mesoporous ZSM-5 (MesZSM-5) and mesoporous ZSM-5 treated with tartaric acid (MesZSM-5\*). All studies were carried out using a pyroprobe reactor. Conditions: 873 K, 19 mg catalyst per mg glucose, and 240 s reaction time. Reprinted from Foster, *et al.* (ref. 94) with permission from the publisher.

Table 5 Summary of product yield and selectivity observed during CFP of lignin residue and maple wood in a fluidized bed reactor. Reaction condition: temperature 873 K, spray dried ZSM-5 catalyst, 0.2 WHSV, 3.2 slpm N<sub>2</sub> fluidization flow rate, and 30 min total reaction time. Yields and selectivity are both reported here on a carbon basis

Compound	Lignin residue	Maple wood
<b>Overall yields</b>		
Carbon monoxide	12.3	24.1
Carbon dioxide	5.8	8.2
Methane	3.1	3.1
Olefins	1.2	7.1
Aromatics	2.2	14.8
Coke	69.0	32.0
Total balance	93.6	89.3
Unidentified	6.4	10.7
<b>Aromatic selectivity</b>		
Benzene	39.6	32.0
Toluene	21.6	43.2
Xylenes	9.45	12.7
Naphthalenes	20.2	5.7
Other aromatics	8.5	6.7
<b>Light hydrocarbon selectivity</b>		
Ethylene	79.2	43.5
Propylene	15.8	52.9
Butenes	5.0	3.6

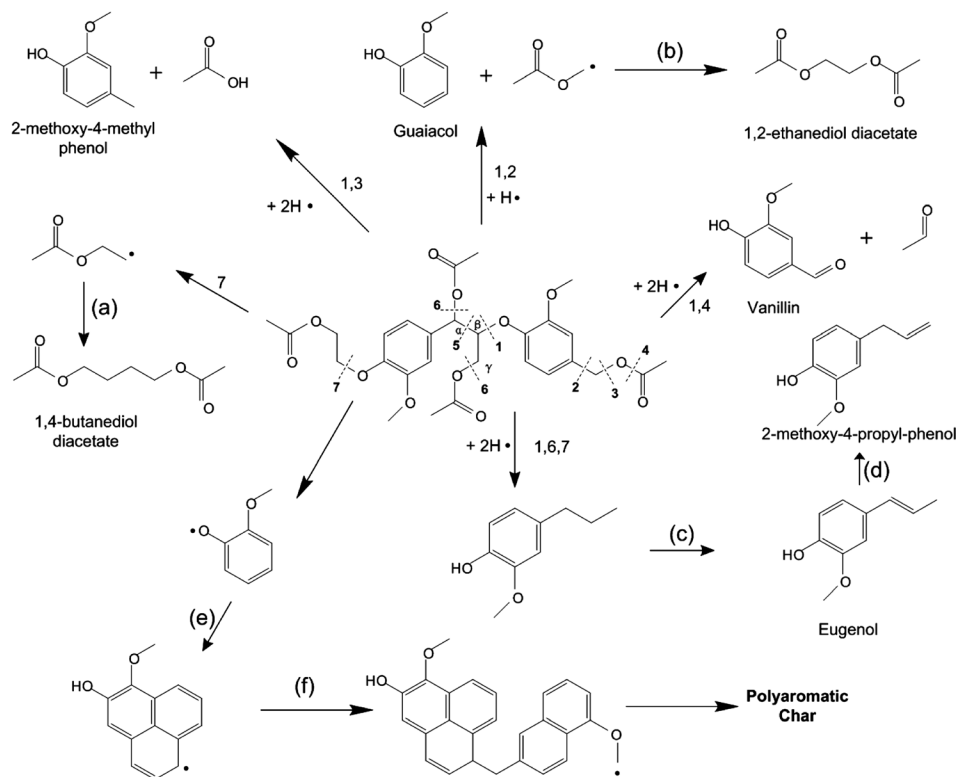


Fig. 12 Proposed reaction pathways occurring during pyrolysis of a lignin model compound. Reproduced from ref. 107.

temperature range (450–700 K) with an apparent activation energy of  $74 \text{ kJ mol}^{-1}$ . In this step, lignin decomposition results in the formation of polyaromatic fragments and light organics. The second step has a higher apparent barrier ( $110 \text{ kJ mol}^{-1}$ ) and becomes dominant at higher temperatures. In this step, the polyaromatic compounds formed in the initial step further decompose into volatile species.<sup>106</sup> Thus, from kinetic studies it was concluded that higher temperatures are favorable for vapor generation during lignin pyrolysis; however, the ability to leverage temperature is limited by the difficulty of delivering sufficiently high heating rates.

To further expand our fundamental understanding of the mechanism of lignin pyrolysis, a model lignin compound was synthesized and characterized in fast pyrolysis experiments.<sup>107</sup> This model compound showed similar thermogravimetric characteristics as plant-based lignin. Fig. 12 shows a proposed mechanism of pyrolysis leading to the formation of 2-methoxy-4-methyl phenol, guaiacol, 1,2-ethanediol diacetate, 1,4-butanediol vanillin, eugenol, and polyaromatic char from the model compound. The proposed mechanism involves formation and reaction of free radicals; as such, controlling product distributions in lignin pyrolysis is exceedingly difficult. Despite CFP offering reasonable aromatic yields from sugars or whole biomass, it is ineffective for converting lignin and humic residues obtained from acid residues in this project. Based on this insight, we conclude that combustion of lignin and humic residues for heat and power production is presently the only workable option for reclaiming some value from solid residuals at distributed scales.

## 4 Economic analysis of the process

In this section, we outline a roadmap for the “best case” jet fuel technology and provide a process model along with economic analysis. As highlighted in the preceding sections, this strategy utilizes red maple as a feedstock and is based upon chemical conversion of the maple through hydrolytic fractionation. In general, fractionation allows for selective processing of specific sugars to deliver linear and branched alkanes, and lignin residues are used as a boiler feed for heat and power production. Our techno-economic analysis of this process is based upon the following assumptions:

1. Process model parameters (yields and selectivities) used to calculate mass balances are based on the experimental data described in the preceding sections of this article.
2. The process can be scaled without a loss in performance. No hydrodynamic constraints are considered in this analysis.
3. Model parameters (residence times and LHSV) from bench scale reactors were used to size process units.
4. Biomass and other raw materials were obtained at costs determined by present market analysis.
5. Other parameters used in developing the economic model are summarized in Table 6.

Fig. 13 outlines the process flow diagram (PFD) for the production of hydrocarbons from air-dried red maple (7.3 wt% moisture). For the techno-economic analysis, we considered a plant that processes 1757 dry MT per day of red maple that are subjected to pretreatment, hydrolysis, and subsequent sugar

Table 6 List of economic parameters used for the economic analysis of the lignocellulosic biorefinery

Category	Parameter	Assumption	
Project financing Assumptions for discounted cash flow analysis	Equity	100	%
	Depreciation method	Variable declining balance (VDB)	
	Depreciation period	7	Years
	Construction period	3	Years
	Discount rate	6.74	%
	Income tax rate	35	%
	Operating hours	8400	Hours per year
	Cost year of analysis	2010	
	Inflation	2	% Per year
	Calculation of fixed costs and working capital	Inside battery limits (ISBL) costs	Estimated from Aspen simulation
Outside battery limits (OSBL) costs		30% of ISBL costs	
Direct costs		ISBL + OSBL costs	
Engineering and supervision		30% Of direct costs	
Construction and fee		30% Of direct costs	
Contingency		20% Of direct costs	
Fixed capital investment		2.34* ISBL costs	
Working capital		5	% of FCI
Important raw material and utility costs	Red maple	51	\$ per MT
	Hydrogen	2000	\$ per MT
	Ru-based catalyst	540	\$ per kg
	Pt/SiO <sub>2</sub> -Al <sub>2</sub> O <sub>3</sub>	2000	\$ per kg
	Amberlyst	150	\$ per kg
	SiO <sub>2</sub> -Al <sub>2</sub> O <sub>3</sub>	5	\$ per kg
	Catalyst refurbishing cost	10% of total catalyst cost per year	
	Waste water treatment	36	\$ per MT
By-product prices for revenue calculations	Acetic acid	772	\$ per MT
	HMF	1580	\$ per MT
	Light ends	2	\$ per gal
	Naptha	2.5	\$ per gal

conversion. This capacity of the plant was selected to be consistent with representative models for distributed scale lignocellulose processing facilities.<sup>39,80,108</sup> The plant consists of three identical process trains operating in parallel, and the performance of one process train was simulated using Aspen Plus<sup>®109</sup> software. The PFD for a process train can be broken into three sections: biomass pretreatment, hemicellulose processing, and cellulose processing.

For biomass pretreatment, optimal cost-effectiveness and process compatibility were demonstrated using hot-water extraction. By scaling the technologies reported here, hot water pretreatment will facilitate roughly 85% recovery of the hemicellulose as aqueous xylooligomers and monomers. Along with xylooligomers and monomers; acid soluble lignin, acetic acid and trace amounts of glucose are also extracted in the aqueous hemicellulose stream (474 MT per day). The remaining inputs are recovered as residual solids (1154 MT per day) comprised of cellulose and lignin, which are utilized in downstream cellulose processing.

Xylooligomers extracted during pretreatment are subsequently converted to linear alkanes in a four-step process comprised of (i) hydrolysis and dehydration of xylooligomers to form furfural, (ii) aldol-condensation of furfural with acetone, (iii) hydrogenation of furfural condensation products to form a C<sub>13</sub> precursor and (iv) hydrodeoxygenation of the C<sub>13</sub> precursor to form *n*-tridecane and other hydrocarbons. In this manner, xylooligomers are converted to linear alkanes (152 MT per day),

corresponding to 80% of the maximum theoretical yield (1.6 kg of xylose can theoretically produce 1 kg of hydrocarbons<sup>34</sup>). The primary loss of selectivity in this approach is attributed to formation of humins during xylose dehydration and loss of furfural to the aqueous stream after biphasic dehydration. Along with the hydrocarbons, chemicals such as acetic acid (76 MT per day) and HMF (31 MT per day) are produced as by-products.

Pretreated solids (cellulose and lignin) are then subjected to dilute acid hydrolysis using 1.5% H<sub>2</sub>SO<sub>4</sub> in a batch reactor. Cellulose is converted to equimolar quantities of levulinic and formic acids, which are recovered in aqueous solution. LA yields on the order of 75% of theoretical were achieved using this approach, corresponding to 350 MT per day of LA and 139 MT per day of FA produced in this strategy.

The primary loss of carbon in this step occurs through formation of humins through condensation of unreacted sugars with dehydration products (such as HMF). Humins and lignin (678 MT per day) are recovered by filtration and combined with residual solids from furfural production (120 MT per day). Given that poor selectivity was observed in catalytic processing of lignin and humic residues, the carbonaceous solids recovered from the process are best suited to combustion, which generates 98 MW of heat. This heat is utilized to provide the process energy requirements using heating oil and high pressure steam.

2-SBP is subsequently added to cellulose hydrolyzates, facilitating extraction and subsequent hydrogenation of LA.

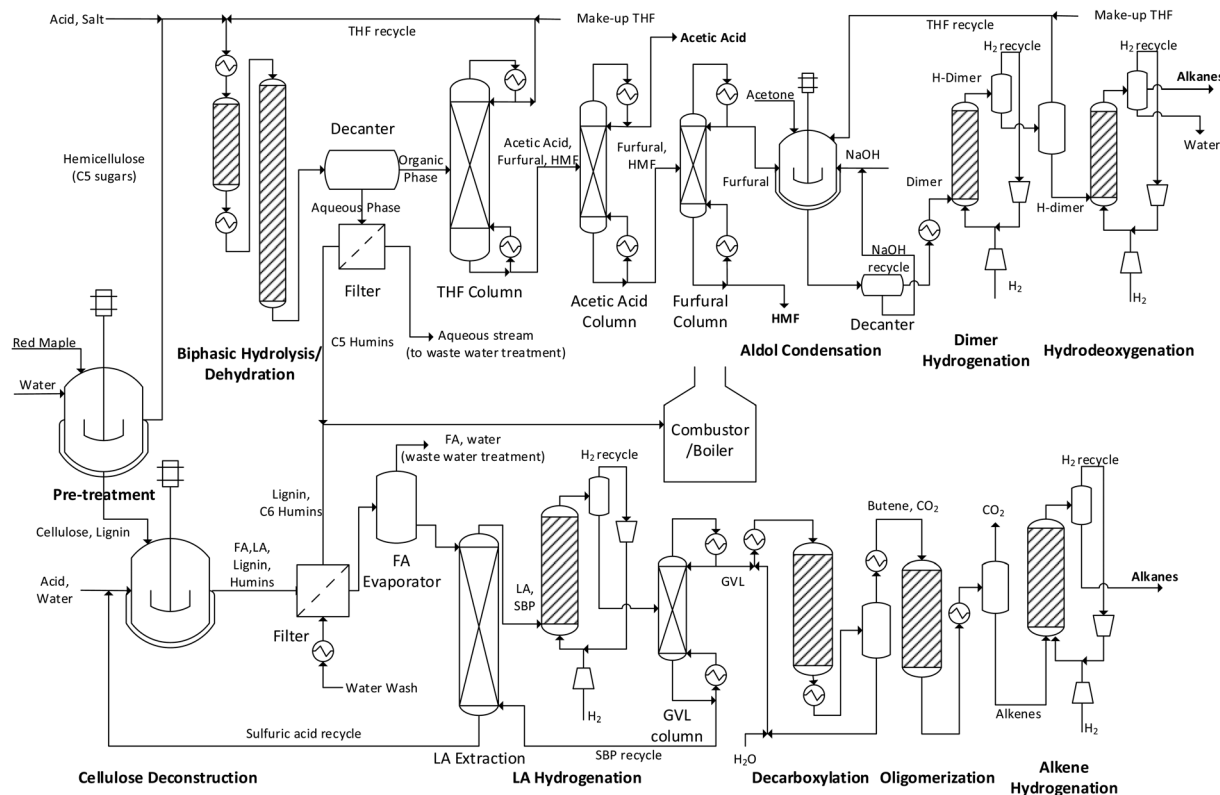


Fig. 13 Simplified process flow diagram for a biorefinery processing red maple as a feedstock for the production of linear hydrocarbons using a hydrolytic fractionation approach.

Because of its poor partition coefficient in SBP, FA is lost in the aqueous stream. Economic models reported here do not consider recovery of FA from cellulose hydrolysis as it was determined not to be cost effective. Instead, most of the FA was evaporated prior to LA extraction to reduce the cost of downstream separation as described by Sen *et al.*<sup>108</sup> Using RuSn/C, LA is converted selectively to GVL (296 MT per day) in the presence of the extracting solvent, and GVL is recovered by distillation. The aqueous phase (containing catalytic sulfuric acid) is recovered quantitatively for subsequent cycles of cellulose hydrolysis. GVL is next diluted to 6 M in water and processed in a two-reactor system. In the initial reactor, it undergoes decarboxylation over  $\text{SiO}_2/\text{Al}_2\text{O}_3$  to form butene isomers (164 MT per day) and carbon dioxide (128 MT per day). In a second reactor, over acidic resins (Amberlyst-70), butenes are converted by oligomerization to branched alkenes in the  $\text{C}_8$ – $\text{C}_{20}$  range. This mixture is then hydrogenated to produce a branched alkane product (165 MT per day). The hydrocarbon products obtained from hemicellulose processing and cellulose processing can be sold as natural gas and propane (3.7 MT per day, 0.8 Mgal per year), naphtha (57.4 MT per day, 7.5 Mgal per year), jet fuel (224 MT per day, 27.5 Mgal per year), and diesel (31 MT per day, 3.1 Mgal per year).

#### 4.1 Overall mass balances

This analysis was carried out using Aspen Plus®<sup>109</sup> simulation software. The reactor mass balances were calculated based on

experimental results, while most separation units were simulated using Aspen models. Where necessary, experimental data were used to augment Aspen models for separation units. For example, laboratory data provided inputs for the design of a biphasic decanter for hemicellulose processing and a liquid extraction column for levulinic acid recovery. Fig. 14 shows the flow of major components across the three parts of the process. The plant processes 1757 MT per day of red maple and delivers the various products described earlier. Apart from the feedstock, the main inputs to the process are water, hydrochloric acid, hydrogen, and acetone. Acetone is required in hemicellulose processing as a reactant for aldol condensation, while hydrogen is required to convert the hydrocarbon precursors to alkane fuels. In cellulose processing, most of the oxygen is removed *via* dehydration or decarboxylation, while in hemicellulose processing a larger portion of the oxygen is removed *via* hydrodeoxygenation. Thus, the hydrogen requirement for hemicellulose processing (20 MT per day) is much higher than cellulose processing (8 MT per day). Makeup quantities of solvents, such as THF and SBP, are additionally required to account for their losses into the wastewater stream. 43 MT per day of HCl and 0.3 MT per day of  $\text{H}_2\text{SO}_4$  are additionally consumed due to inefficiencies in separation and recycle of these homogeneous catalysts. Lignin and  $\text{C}_6$  humins from cellulose processing (678 MT per day) and  $\text{C}_5$  humins from hemicellulose processing (120 MT per day) are combusted to provide 98 MW of heat. This heat is utilized in various applications and exceeds the total energy requirement of the process.

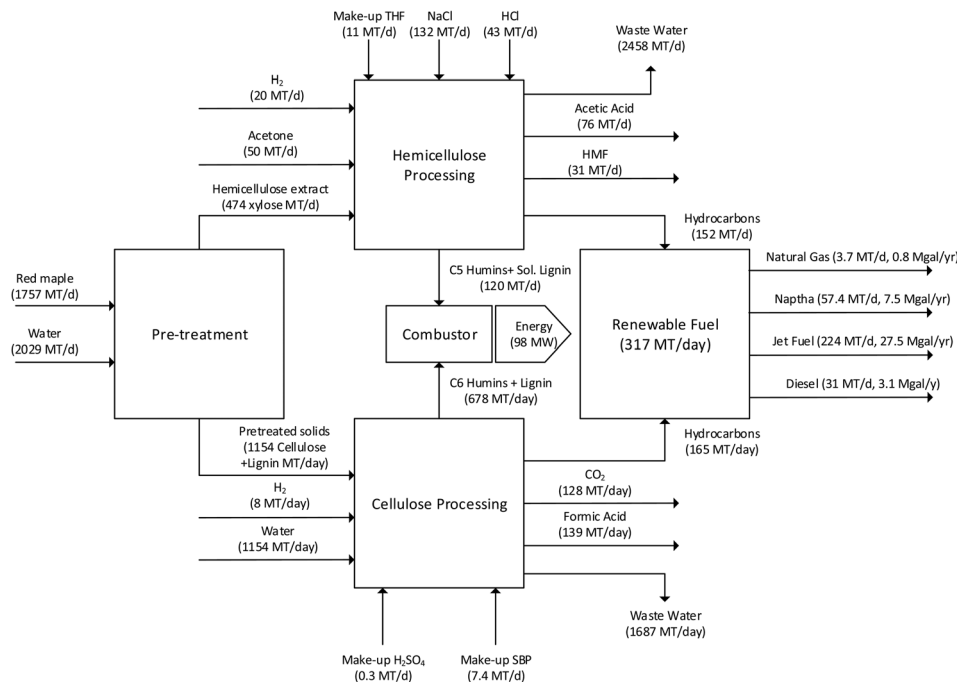


Fig. 14 Overall input–output analysis for different processing units in lignocellulosic biorefinery.

Apart from these streams, 4145 MT per day of waste water is also generated and must be processed in a wastewater treatment facility.

## 4.2 Equipment sizing and cost

Table 7 summarizes major equipment costs for this biorefinery. Experimental data were used to size various reactors with an assumption that the process can be scaled without a loss in performance. Materials of construction were selected based on the following criteria: monel was used with highly acidic environments at high temperatures, stainless steel with molybdenum (SS6Mo) was used in mildly acidic moderate conditions, and SS316 was used for all other equipment. Equipment size and cost were determined using Aspen Process Economic Analyzer<sup>®110</sup> software (APEA). The amount of heterogeneous catalyst required were calculated based on experimental data.<sup>36,37,57</sup> Based on unit catalyst cost values given in Table 6, the catalyst costs for the biorefinery were estimated. Table 7 gives the sizing information for the major equipment used in the process. The major capital costs were contributed by reactors and the catalysts (\$85.2 M, 41% of total capital cost), compressors and pumps (\$44.0 M, 21% of total capital cost) and a combustor/boiler (\$32.9 M, 16% of total capital cost). Heterogeneous catalyst costs corresponded to 50% of the total catalyst and reactors costs. Distillation and extraction columns accounted for 9% of the total equipment cost, and various heat exchangers—in aggregate—accounted for 7% of the total cost. The total equipment cost for the plant was calculated to be \$208.8 M. The equipment costs obtained from the APEA<sup>110</sup> were used to calculate inside battery limits (ISBL) costs for the plant.

## 4.3 Operating costs

A summary of operating costs is given in Table 8. Operating costs were divided into raw material costs, solvent costs, and catalyst refurbishing costs, and utility costs for 350 days of operation annually. Red maple is the primary raw material expense at \$31.4 M per year (22% of annual operating costs). Acetone (\$19.1 M per year, 14% of annual operating costs) and hydrogen (\$20.0 M per year, 14% of annual operating costs) are additionally significant operating expenses. Assuming 10% catalyst is refurbished every year, the catalyst refurbishing costs were calculated as \$4.3 M per year. Refurbishing heterogeneous catalysts (\$4.3 M per year) and replenishing THF (\$5.5 M per year), HCl (\$3.8 M per year), and NaCl (\$1.6 M per year) contribute, in total, 11% of the annual operating expenses, whereas make up of SBP and H<sub>2</sub>SO<sub>4</sub> are negligible. All of the energy consumption in the two main process utilities, waste water treatment and heat and power generation, is satisfied by combustion of lignin and humic residues generated internally. The process generates 4145 MT of wastewater per day, which is treated prior to discharge and will account for 38% of annual operating costs. Considering all of the aforementioned, total operating expenses are calculated to be \$138.9 M per year.

## 4.4 Economic assessment of current process

We analyzed the economic viability of the proposed process using the conceptual process design approach developed by Douglas.<sup>111–113</sup> Based on this methodology and the ISBL costs, the total fixed capital investment for the plant was estimated to be \$467 M. Table 6 gives the list of assumptions made for calculating the minimum selling price of hydrocarbons using this

Table 7 Summary of estimated capital costs for equipment required in the process described here

Sr. No	Equipment	# of units	T (K)	P (atm)	Heat duty (kW per reactor)	Sizing details			Catalyst costs (\$)	Equipment cost (\$)
						Vol. (m <sup>3</sup> )	D (m)	MOC		
1	Reactors and catalyst systems	78								85 160 096
1.1	Pretreatment	6	473	16	138	9.32	1.8	Monel		4 175 400
1.2	Biphasic hydrolysis/dehydration	15	384/473	54	1	4.4/8.6	1/1.3	SS6Mo		15 654 300
1.3	Aldol condensation	3	309	1	-660	9.90	1.8	Monel		1 950 000
1.4	Dimer hydrogenation	3	383	54	660	5.81	1.1	SS6Mo	5 893 965	7 113 765
1.5	Hydrodeoxygenation	9	523	61	-1060	9.53	1.3	SS316	24 091 232	25 825 532
1.6	Cellulose deconstruction	6	473	16	-296	27.84	2.6	Monel		5 898 300
1.7	LA hydrogenation	15	493	35	-146	5.70	1.1	SS6Mo	3 803 809	6 689 809
1.8	Decarboxylation	15	648	36	52.5	8.53	1.3	SS316	400 500	5 470 500
1.9	Oligomerization	9	443	35	-270	9.12	1.3	SS316	6 977 045	10 158 545
1.10	Alkene hydrogenation	3	423	34	-426	1.66	0.8	SS316	1 680 345	2 223 945
2	Distillation and extraction columns	12								18 848 100
2.1	THF column	3	366/477	3		40 stages		SS6Mo		8 420 100
2.2	Acetic acid column	3	415/466	2		26 stages		SS6Mo		2 778 900
2.3	Furfural column	3	449/546	2		12 stages		SS316		1 493 400
2.4	LA extraction column	3	454			20 stages		SS6Mo		633 900
2.5	GVL distillation column	3	393/512	1		23 stages		SS6Mo		5 521 800
3	Combustor/boiler	1								32 913 135
4	Compressors and pumps									43 971 000
5	Separation vessels and filters									12 926 700
6	Heat exchangers									15 012 900
	Total equipment cost									208 831 931

process. The project is 100% equity financed with a depreciation period of 7 years. The construction period for the plant was assumed to be 3 years. Working capital was estimated to be 5% of the total capital investment. The market discount rate was taken as 6.74%,<sup>39,80,108</sup> and the income tax rate was taken as 35%. Other parameters include an inflation rate of 2% per year. By-products are additionally assumed to be saleable at market

price, which was based on present values for acetic acid (\$772 per MT), HMF (\$1580 per MT), light hydrocarbons (*i.e.* natural gas and LPG at \$2 per gal), and naphtha (\$2.5 per gal).<sup>114,115</sup> A discounted cash flow analysis was then carried out for a plant lifetime of 20 years.<sup>115</sup> The selling price of distillate fuels were adjusted to obtain a zero net present value of the project. From this economic analysis, we calculate minimum selling prices for distillate fuels (*i.e.* jet and diesel fuels) as \$4.75 per gallon.

Table 8 Summary of operating costs involved in the processing of lignocellulosic biomass to hydrocarbons

Sr. no.	Inputs	Requirement	Unit cost	Total cost
	Raw material/utility	(MT per year)	(\$ per MT)	(\$ per year)
	Raw materials			70 458 885
1	Red maple	614 775	51	31 353 525
2	Acetone	17 364	1102	19 139 960
3	Hydrogen	9983	2000	19 965 400
	Solvents/catalyst/additive			15 328 300
1	THF	1613	3417	5 511 881
2	SBP	2596	50	129 800
3	HCl	15 120	250	3 780 000
4	NaCl	46 040	35	1 611 400
5	H <sub>2</sub> SO <sub>4</sub>	117	90	10 530
6	Heterogeneous catalyst refurbishing <sup>a</sup>			4 284 690
	Utilities			53 154 279
1	Electricity <sup>b</sup>	17 085 897	0.054	922 638
2	Waste water	1 450 879	36	52 231 641
	Total operating costs			138 941 464

<sup>a</sup> 10% of the heterogeneous catalyst is assumed to be refurbished every year. <sup>b</sup> Electricity requirement is in kW h and cost is the unit: \$ kW<sup>-1</sup> h<sup>-1</sup>.

The technoeconomic evaluation results are summarized in a Sankey diagram shown in Fig. 15. This Sankey diagram shows the flow of carbon through various processing units of the biorefinery. The height of each stream corresponds to the amount of carbon in the stream, while the darkness of the stream represents the carbon concentration in the carbon precursor molecule. As seen from the figure, the streams become progressively darker representing removal of oxygen and concentration of carbon in the precursor molecules. The major loss of carbon occurs as lignin and humins. Most of these humins are produced during LA production. For simplicity, flow of water, homogenous catalysts and solvents is not included in the figure. In addition to representing the material flows, the capital costs associated with a unit operation is represented by the height of the unit block. Hence, as seen from the figure, hydrodeoxygenation reactor is the most capital intensive unit, mainly due to the high cost of precious metal catalysts.

#### 4.5 Recommendations for further cost reduction

From the technoeconomic analysis and as highlighted in Fig. 15, there are several areas where future research efforts should be focused to reduce the cost. These areas include: (1)

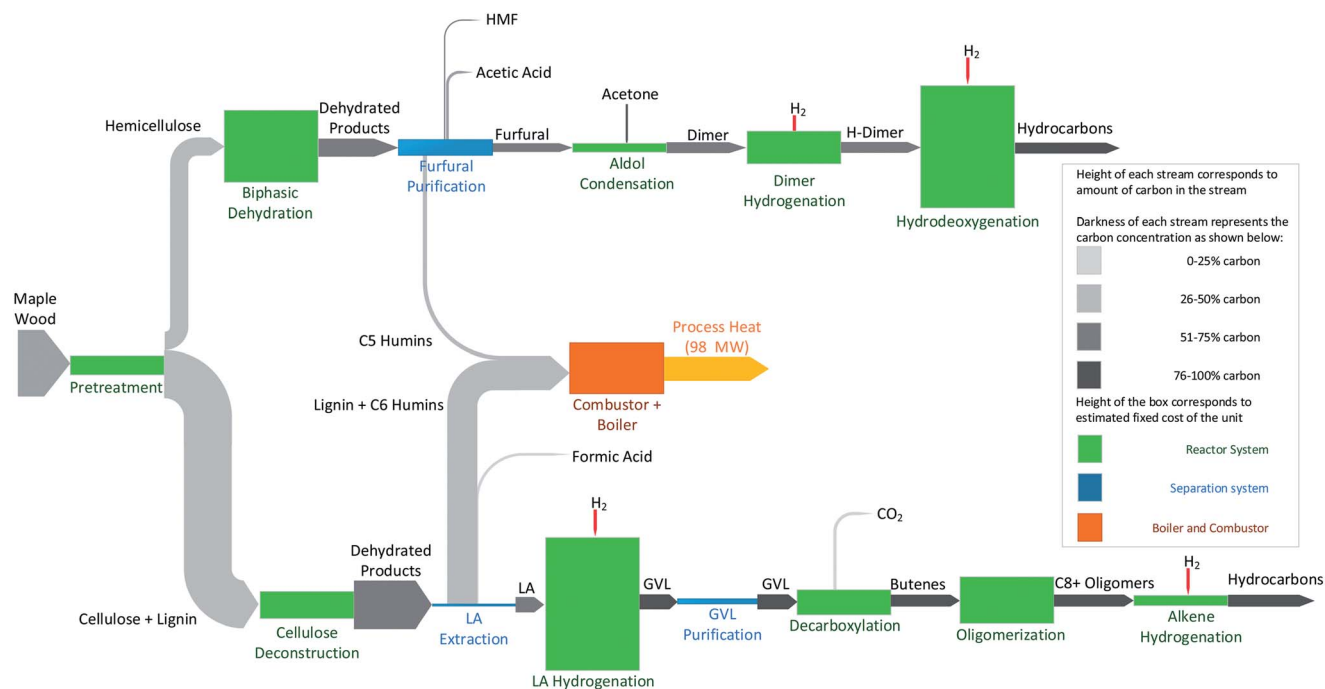


Fig. 15 Sankey diagram based on carbon balance of the lignocellulosic biorefinery representing flows of carbon in major streams of the process.

decreasing catalyst cost for the hydrodeoxygenation reactor: the current hydrodeoxygenation reactor utilizes expensive Pt-based catalysts which results in high catalyst costs for the reactor. With cheaper base metal catalysts in this step, the capital cost for hydrodeoxygenation unit can be lowered substantially. This is one of the most promising approach for cost reduction. Base metal catalysts such as sulfided Ni–Mo catalysts have been tested in the literature for such reaction which could potentially be used for this reactor.<sup>116,117</sup> If platinum is replaced by cheaper base metal catalyst for hydrodeoxygenation, the minimum selling price of the jet fuel will go down by 5%. (2) Lignin and Humins conversion: in the current approaches described in this paper, about 45% of the carbon present in the biomass ends up as lignin and humic residues. Although in this process these residues are combusted to recover energy for the process, considerable economic benefits can be achieved if lignin is converted to useful fuels or chemicals. Lignin conversion is one of the heavily researched areas in biomass conversion<sup>118–120</sup> and any advances in this field will greatly improve the economic feasibility of biofuels projects. (3) Low yields of LA acid and low xylose recoveries: currently, we are able to obtain only 75% of theoretical yield of levulinic acid. Thus, large amount of carbon is lost as humins in this step which results in low overall efficiencies. Hence, improving yields of LA will improve the carbon yields of the process. Although, it must be noted that, in the current yield of 75% was obtained after detailed study of reaction kinetics. Hence, with the existing process, it is less likely to improve the yields further. Also, currently we are obtaining about 85% xylose recoveries in hot water extraction. This represents one of the lowest yield steps in hemicellulose conversion. Thus, future technologies should focus on improving the recovery of xylose from pretreatment processes.

In addition to these areas, one of the major operating costs for the biorefinery is the waste water treatment. For every kg of biomass processed, the biorefinery generates 2.36 kg of waste water. Hence, the waste water treatment costs are higher than the biomass costs for the biorefinery. This makes the technology infeasible in locations where there is scarcity of water. Currently, to maintain high yields of furfural in the process lower concentration *i.e.* larger volumes of water are needed. Also, salt added to improve the partitioning makes the aqueous phase unsuitable for recycle. Thus, development of technologies which enable recycle of water are necessary to improve the economics and reduce the requirements on the process. With improved recycle structure of water stream, considering waste water stream generated only during reactions, the minimum selling price of the biorefinery will go down drastically to \$3.11 per gallon.

In the current state, this hydrolysis based upgrading approach does not compete favorably with fast pyrolysis-hydrotreating based approach discussed by researchers at Iowa State, National Renewable Energy Laboratories (NREL) and Conoco-Phillips.<sup>31,121</sup> Although it should be noted that there are several technological challenges associated with fast pyrolysis-hydrotreating including catalyst deactivation and coking, indicating that the economic analysis made by the Iowa State team is overly optimistic.<sup>116,117,122</sup> This same team has also published technoeconomic analyses on other biofuels technologies such as ethanol production<sup>123</sup> and gasification–Fischer–Tropsch synthesis.<sup>124</sup> However most of these studies do not consider the integrated approach between various unit operations and effect of impurity carryover in downstream processing. Thus, more advances in these fields are necessary to improve these models further for fair comparison. Recently, Maravelias and

co-workers have calculated similar minimum selling prices with hydrolysis-based upgrading processes.<sup>49,80,108,125</sup> These studies do not utilize separate processes for conversion of cellulose and hemicellulose. Also, these studies are based on lower yields of LA production from cellulose (55–61% compared to 75% in this study) and furfural from hemicellulose (56% compared to 85% in this study). As a result, the approach described in this paper presents higher yields of end products compared to these previous studies. We believe that future advances in designing cheaper base metal catalysts, improving the water recyclability, and converting the lignin into fuels will decrease the costs to where the process described in this paper could become economically viable.

## 5 Conclusions

This project yielded both fundamental and applied technological principles valuable for the design of a process for the catalytic production of alkane fuels from lignocellulosic biomass and successfully demonstrated an integrated process for conversion of hardwoods into hydrocarbons and commodity chemicals. Further, utilization of lignocellulose-derived feedstocks throughout the project enabled consideration of critical issues, such as impurity carryover and process compatibility, which are not typically included in model studies. Coupling pretreatment with downstream upgrading has revealed that hot water extraction is the most effective method when targeting production of furfural and levulinic acid from a single biomass source. We have additionally observed that both levulinic acid and furfural can be transformed into higher alkanes *via* cascade processing, and that jet fuel-range alkanes can be produced in this manner at a minimum selling price of roughly \$4.75 per gallon. Low lignin pyrolysis yields indicate that the most likely application for lignin and humins is direct combustion. Opportunities for further cost reduction indicate that the cost of this process could be reduced to a minimum selling price of \$4.52 per gallon assuming that base metals can replace the precious metals for hydrodeoxygenation. Also, with improved recyclability of water in the process, the minimum selling price of the jet fuel can be drastically reduced to \$3.11 per gallon.

Considering only demonstrated selectivities in chemical transformations, hemicellulose from red maple can be converted into C<sub>13</sub>–C<sub>31</sub> alkanes with carbon yields approaching 80% of the theoretical maximum; however, interstage separations will decrease carbon yields in real implementation, and our overall analysis suggests a 60–65% carbon yield of alkane products from hemicellulose. From a chemical perspective, the primary loss of carbon in hemicellulose upgrading is associated with incomplete extraction of sugars during pretreatment (85% recovery), and we anticipate that this can be improved *via* further optimization of hot water extraction. All reactions downstream of hemicellulose extraction are carried out at nearly quantitative yields. As such, any improvement in pretreatment yields will translate directly to an improvement in total carbon yields in the hemicellulose upgrading scheme.

External supplies of acetone and THF required for furfural production and upgrading lead to high operating costs

associated with xylose upgrading. The supply of an external ketone for condensation is not easily avoided in jet fuel production; however, future strategies might consider internal production of acetone (for example, by ketonization of acetic acid) to offset this expense. While acetic acid sales help to reduce the minimum alkane selling price, acetic acid markets may not absorb output commensurate with large scale production of lignocellulosic fuels. Acetic acid could instead be converted to acetone to decrease external acetone demand in furfural condensation. Replacement of THF lost to the aqueous phase during biphasic furfural production is another significant operating expense. Though this system delivers molar furfural yields in excess of 90%, THF makeup will likely become problematic at large scales. Alternative solvents are unlikely to significantly improve furfural yields, but a less water-soluble solvent that partitions furfural comparably to THF could significantly reduce operating costs.

Cellulose hydrolysis efforts have revealed that both stirred tank and steam gun reactors can deliver 70–75% molar yields of levulinic and formic acids from red maple using minimal acid loadings (1.5 wt%). Importantly, steam gun reactors permit increased solid loadings (50 wt%), increasing LA concentrations while reducing mineral acid concentrations in raw cellulose hydrolyzates. Extensive research on LA upgrading has revealed that  $\gamma$ -valerolactone is likely the most versatile LA derivative when targeting jet fuel production. GVL is produced *via* hydrogenation of LA over Ru-based catalysts with high yields at short residence times. To date, the greatest impediment to large scale GVL production is the sensitivity of the Ru catalyst to residual mineral acids and soluble lignin fragments in the LA feed. As a result, LA purification may represent a prohibitive cost in this strategy. A novel alkylphenol solvent system was found to be effective at removing such poisons from the LA stream, expediting the production of GVL. Once obtained, GVL undergoes decarboxylation over SiO<sub>2</sub>–Al<sub>2</sub>O<sub>3</sub> to form butenes, which are subsequently oligomerized over an acidic resin to yield branched, distillate-range hydrocarbons. Though the present cost of GVL production prohibits its use for alkane fuel production, economic models suggest that at distributed processing scales, lignocellulosic GVL could be produced cheaply enough to make the decarboxylation route viable for targeting production of synthetic aviation fuels.

The cellulose fraction of red maple can be converted into jet fuel range alkanes at roughly 70% of the theoretical maximum. In this scheme, the limiting yield is associated with levulinic acid production *via* dilute acid hydrolysis (75% of theoretical), and the main loss of selectivity is associated with humin formation. Further improvements in LA yields will translate directly to reduced red maple consumption, significantly impacting the minimum selling price of alkane fuels. We anticipate that improved understanding of degradation pathways may help improve LA yield. If humin formation during acid hydrolysis can be well described, it will enable the design of reactive systems that minimize the loss of cellulose to degradation pathways. We note that 70% of the maximum theoretical yield of alkanes corresponds to roughly 50% recovery of the carbon in cellulose. However, maximal carbon yields are limited

in this strategy because two of the carbon atoms in the parent glucose are lost as formic acid (during HMF decomposition) and CO<sub>2</sub> (during GVL decarboxylation). Neither of these products is directly incorporated into the alkane fuel; thus, they are not counted here toward product carbon yields; however, formic acid can be leveraged for internal H<sub>2</sub> production, and decarboxylation facilitates oxygen removal without hydrogen addition. Thus, the relatively low carbon yields in the cellulose processing scheme are balanced by reduced hydrogen consumption.

Despite extensive consideration of lignin and humin upgrading, no cost effective strategies were identified. Catalytic Fast Pyrolysis is an attractive technology for producing olefins and aromatic monomers from carbohydrates and whole biomass, but it is less effective for depolymerisation of lignin or humic residues. Though niche applications for lignin are becoming increasingly common (*e.g.*, resins, specialty chemicals), the field would benefit from a commodity-scale lignin application beyond heat and power, and efficient production of aromatic monomers is particularly desirable. To this end, studies focusing on lignin/humin structure and mechanisms of formation and depolymerization could help direct future efforts for the upgrading lignin fractions.

Although novel chemistries, reactor configurations, and strategies for process intensification were developed through this program, the most significant outcome was the integration of formerly isolated technologies to deliver jet-fuel range alkanes directly from red maple. Impurities and residuals from lignocellulose depolymerisation hinder downstream catalytic conversion, and intensive purification efforts are required to maintain high catalytic activity, particularly in cellulose processing. Experimental results verify that each individual step can be carried out in good yield; however, interstage separation, purification, and product recovery are cumbersome and have manifested in reduced carbon yields in product alkanes derived from red maple. Future efforts must therefore focus not only on the basic chemistry of biomass conversion, but also on developing effective, less economically intensive strategies for product recovery. Improved separation strategies could drastically decrease operating costs by reducing solvent consumption and energy demand. Further, identifying feedstock impurities responsible for catalyst deactivation will allow the design of stable materials and processes. Employing deactivation-resistant catalysts will alleviate stringent requirements for feedstock purity and ultimately enable intensified processes delivering equivalent yields with reduced separations burdens.

A final consideration is the substantial cost of wastewater treatment associated with this technology. The large volume of water that must be treated is directly related to the relatively low concentrations of sugars and platform intermediates obtained during pretreatment and hydrolysis. Low concentration processing appears necessary in some cases such as furfural production, where excessive sugar concentrations lead to uncontrolled humin formation, but we generally expect that processing dilute streams leads to low rates of reaction, large reactor volumes, and unnecessary energy consumption in process heating, separations, and water treatment. Further,

excessive water consumption can prohibit adoption of the technology, particularly where the large-scale cultivation of biomass feedstocks is already likely to strain water supplies. For these reasons, it is important to envision processes that can accommodate higher concentrations of sugars and/or platform intermediates in the aqueous phase. This will decrease both water consumption and the significant costs associated with water treatment.

To summarize, the processes detailed here are demonstrated to deliver high yields of alkane fuels from hemicellulose and cellulose derived from red maple. Future efforts directed toward improving yields from key transformations such as pretreatment, cellulose hydrolysis, and lignin depolymerisation will decrease raw material costs and improve total carbon yields. Another important set of biorefining challenges is interfacing conversion technologies that have been previously considered in isolation.<sup>126</sup> Our attempt to integrate the numerous technologies required to transform red maple into aviation fuels highlights the need for streamlined separations, increasingly robust catalytic materials, and intensified processes. We consider that this technology is a strategic approach to biorefining that specifically targets distillate-range alkanes, addressing the long term need of securing heavy fuels from renewable resources.

## Acknowledgements

The experimental work was supported by the Defense Advanced Research Project Agency (DARPA) through the Defense Science Office Cooperative Agreement W911NF-09-2-0010 (SurfCat: catalysts for production of JP-8 range molecules from lignocellulosic biomass. Approved for Public Release, Distribution Unlimited). Work on process design and simulation, and costing is carried out at Massachusetts Institute of Technology under Projects 28 and 47 of the Partnership for Air Transportation Noise and Emissions Reduction (PARTNER), and funded by the Federal Aviation Administration (FAA), Air Force Research Laboratory (AFRL) and the Defense Logistics Agency Energy (DLA Energy). H. O., R. M. and S. R. H. B. would like to thank Dr James Hileman at the FAA for critical and helpful remarks. S. Murat Sen was supported by the DOE Great Lakes Bioenergy Research Center (DOE BER Office of Science DE-FC02-07ER64494). The views, opinions, and findings contained in this article are those of the authors and should not be interpreted as representing the official views or policies, either expressed or implied, of the DARPA, Department of Defense, FAA, AFRL, DLA Energy or DOE.

## References

- 1 C. H. Christensen, J. Rass-Hansen, C. C. Marsden, E. Taarning and K. Egeblad, *ChemSusChem*, 2008, **1**, 283–289.
- 2 R. Repice, R. Adler, J. Berry, J. Michaels, R. Schmitt, R. F. King, N. Paduano, D. Bonnar, A. Lee, A. Barrick, M. Anderson, A. Sweeney, P. Young, C. Wirman, M. Mobilia, G. Jacobs, P. Lindstrom and N. Ko, *Annual*

- Energy Review*, United States Energy Information Administration, Washington, D.C., 2010.
- 3 BP Statistical Review of World Energy, *British Petroleum*, 2012.
  - 4 *U.S. Energy Independence and Security Act*, 2007.
  - 5 G. W. Huber and B. E. Dale, *Sci. Am.*, 2009, **301**, 52–59.
  - 6 R. D. Perlack and B. J. Stokes, *U.S. Billion-Ton Update: Biomass Supply for a Bioenergy and Bioproducts Industry*, U.S. Department of Energy, 2011.
  - 7 Y. Lin and S. Tanaka, *Appl. Microbiol. Biotechnol.*, 2006, **69**, 627–642.
  - 8 N. Qureshi and T. C. Ezeji, *Biofuels, Bioprod. Biorefin.*, 2008, **2**, 319–330.
  - 9 E. L. Kunkes, D. A. Simonetti, R. M. West, J. C. Serrano-Ruiz, C. A. Gartner and J. A. Dumesic, *Science*, 2008, **322**, 417–421.
  - 10 N. Li, G. A. Tompsett and G. W. Huber, *ChemSusChem*, 2010, **3**, 1154–1157.
  - 11 N. Li, G. A. Tompsett, T. Zhang, J. Shi, C. E. Wyman and G. W. Huber, *Green Chem.*, 2011, **13**, 91–101.
  - 12 E. I. Gürbüz, D. M. Alonso, J. Q. Bond and J. A. Dumesic, *ChemSusChem*, 2011, **4**, 357–361.
  - 13 H. Joshi, B. R. Moser, J. Toler, W. F. Smith and T. Walker, *Biomass Bioenergy*, 2011, **35**, 3262–3266.
  - 14 P. J. Fagan and L. E. Manzer, *US Pat.*, 7 153 996, 2006.
  - 15 I. T. Horvath, H. Mehdi, V. Fabos, L. Boda and L. T. Mika, *Green Chem.*, 2008, **10**, 238–242.
  - 16 H. Heeres, R. Handana, D. Chunai, C. B. Rasrendra, B. Girisuta and H. J. Heeres, *Green Chem.*, 2009, **11**, 1247–1255.
  - 17 L. Deng, J. Li, D. M. Lai, Y. Fu and Q. X. Guo, *Angew. Chem., Int. Ed.*, 2009, **48**, 6529–6532.
  - 18 Z. P. Yan, L. Lin and S. Liu, *Energy Fuels*, 2009, **23**, 3853–3858.
  - 19 L. Deng, Y. Zhao, J. A. Li, Y. Fu, B. Liao and Q. X. Guo, *ChemSusChem*, 2010, **3**, 1172–1175.
  - 20 H. Mehdi, V. Fabos, R. Tuba, A. Bodor, L. T. Mika and I. T. Horvath, *Top. Catal.*, 2008, **48**, 49–54.
  - 21 I. Ahmed, *US Pat.*, 7 064 222, 2006.
  - 22 Annual Energy Outlook 2013, *Energy Information Administration*, Washington, DC, 2013.
  - 23 J. R. Regalbuto, *Biofuels, Bioprod. Biorefin.*, 2011, **5**, 495–504.
  - 24 P. N. R. Vennestrøm, C. M. Osmundsen, C. H. Christensen and E. Taarning, *Angew. Chem., Int. Ed.*, 2011, **50**, 10502–10509.
  - 25 D. B. Agusdinata, F. Zhao, K. Ileleji and D. DeLaurentis, *Environ. Sci. Technol.*, 2011, **45**, 9133–9143.
  - 26 D. M. Alonso, J. Q. Bond and J. A. Dumesic, *Green Chem.*, 2010, **12**, 1493–1513.
  - 27 G. W. Huber, R. D. Cortright and J. A. Dumesic, *Angew. Chem., Int. Ed.*, 2004, **43**, 1549–1551.
  - 28 G. W. Huber, S. Iborra and A. Corma, *Chem. Rev.*, 2006, **106**, 4044–4098.
  - 29 G. W. Huber and J. A. Dumesic, *Catal. Today*, 2006, **111**, 119–132.
  - 30 G. W. Huber, J. N. Chheda, C. J. Barrett and J. A. Dumesic, *Science*, 2005, **308**, 1446–1450.
  - 31 M. M. Wright, D. E. Daugaard, J. A. Satrio and R. C. Brown, *Fuel*, 2010, **89**(suppl. 1), S2–S10.
  - 32 T. Zhang, R. Kumar and C. E. Wyman, *Carbohydr. Polym.*, 2013, **92**, 334–344.
  - 33 R. Xing, W. Qi and G. W. Huber, *Energy Environ. Sci.*, 2011, **4**, 2193–2205.
  - 34 R. Xing, A. V. Subrahmanyam, H. Olcay, W. Qi, G. P. van Walsum, H. Pendse and G. W. Huber, *Green Chem.*, 2010, **12**, 1933–1946.
  - 35 S. G. Wettstein, J. Q. Bond, D. M. Alonso, H. N. Pham, A. K. Datye and J. A. Dumesic, *Appl. Catal., B*, 2012, **117–118**, 321–329.
  - 36 D. M. Alonso, S. G. Wettstein, J. Q. Bond, T. W. Root and J. A. Dumesic, *ChemSusChem*, 2011, **4**, 1078–1081.
  - 37 J. Q. Bond, D. M. Alonso, D. Wang, R. M. West and J. A. Dumesic, *Science*, 2010, **327**, 1110–1114.
  - 38 T. R. Carlson, Y. T. Cheng, J. Jae and G. W. Huber, *Energy Environ. Sci.*, 2011, **4**, 145–161.
  - 39 A. R. Aden, M. Ibsen, K. Jechura, J. Neeves, K. Sheehan, J. Wallace, B. Montague, L. Slayton and A. Lukas, *J. Lignocellulosic Biomass to Ethanol Process Design and Economics Utilizing Co-Current Dilute Acid Prehydrolysis and Enzymatic Hydrolysis for Corn Stover*, Report TP-510–32438, NREL, Golden, CO, 2002.
  - 40 D. Lee, V. N. Owens, A. Boe and P. Jerenyama, *Composition of Herbaceous Biomass Feedstocks*, 2007.
  - 41 D. Shallom and Y. Shoham, *Curr. Opin. Microbiol.*, 2003, **6**, 219–228.
  - 42 B. Girisuta, L. Janssen and H. Heeres, *Ind. Eng. Chem. Res.*, 2007, 1696–1708.
  - 43 C. Chang, X. Ma and P. Cen, *Chin. J. Chem. Eng.*, 2009, 835–839.
  - 44 R. Kumar and C. E. Wyman, *Carbohydr. Res.*, 2008, **343**, 290–300.
  - 45 X. J. Shao and L. Lynd, *Bioresour. Technol.*, 2013, **130**, 117–124.
  - 46 N. Mosier, C. E. Wyman, B. E. Dale, R. T. Elander, Y. Y. Lee, M. Holtzapple and M. R. Ladisch, *Bioresour. Technol.*, 2005, **96**, 673–686.
  - 47 M. C. Gray, A. O. Converse and C. E. Wyman, *Appl. Biochem. Biotechnol.*, 2003, **105–108**, 179–193.
  - 48 M. C. Gray, A. O. Converse and C. E. Wyman, *Ind. Eng. Chem. Res.*, 2007, **46**, 2383–2391.
  - 49 D. J. Braden, C. A. Henao, J. Heltzel, C. T. Maravelias and J. A. Dumesic, *Green Chem.*, 2011, **13**, 1755–1765.
  - 50 T. Miyazawa, S. Koso, K. Kunimori and K. Tomishige, *Appl. Catal., A*, 2007, **329**, 30–35.
  - 51 M. Osada, N. Hiyoshi, O. Sato, K. Arai and M. Shirai, *Energy Fuels*, 2008, **22**, 845–849.
  - 52 F. Jin and H. Enomoto, *Energy Environ. Sci.*, 2011, **4**, 382–397.
  - 53 A. A. Peterson, F. Vogel, R. P. Lachance, M. Froling, J. M. J. Antal and J. W. Tester, *Energy Environ. Sci.*, 2008, **1**, 32–65.
  - 54 N. Li and G. W. Huber, *J. Catal.*, 2010, **270**, 48–59.
  - 55 G. Li, N. Li, Z. Wang, C. Li, A. Wang, X. Wang, Y. Cong and T. Zhang, *ChemSusChem*, 2012, **5**, 1958–1966.
  - 56 J. N. Chheda and J. A. Dumesic, *Catal. Today*, 2007, **123**, 59–70.

- 57 H. Olcay, A. V. Subrahmanyam, R. Xing, J. Lajoie, J. A. Dumesic and G. W. Huber, *Energy Environ. Sci.*, 2013, **6**, 205–216.
- 58 A. Corma, O. de la Torre and M. Renz, *Energy Environ. Sci.*, 2012, **5**, 6328–6344.
- 59 A. Corma, O. de la Torre and M. Renz, *ChemSusChem*, 2011, **4**, 1574–1577.
- 60 A. Corma, O. de la Torre, M. Renz and N. Villandier, *Angew. Chem., Int. Ed.*, 2011, **50**, 2375–2378.
- 61 R. Xing, A. V. Subrahmanyam, H. Olcay, W. Qi, G. P. van Walsum, H. Pendse and G. W. Huber, *Green Chem.*, 2010, **12**, 1933–1946.
- 62 R. Weingarten, J. Cho, W. C. Conner and G. W. Huber, *Green Chem.*, 2010, **12**, 1423–1429.
- 63 J. N. Chheda, G. W. Huber and J. A. Dumesic, *Angew. Chem., Int. Ed.*, 2007, **46**, 7164–7183.
- 64 J. N. Chheda, Y. Roman-Leshkov and J. A. Dumesic, *Green Chem.*, 2007, **9**, 342–350.
- 65 K. M. Dooley, A. K. Bhat, C. P. Plaisance and A. D. Roy, *Appl. Catal., A*, 2007, **320**, 122–133.
- 66 M. Renz, *Eur. J. Org. Chem.*, 2005, **6**, 979–988.
- 67 C. A. Gaertner, J. C. Serrano-Ruiz, D. J. Braden and J. A. Dumesic, *J. Catal.*, 2009, **266**, 71–78.
- 68 R. M. West, Z. Y. Liu, M. Peter, C. A. Gartner and J. A. Dumesic, *J. Mol. Catal. A: Chem.*, 2008, **296**, 18–27.
- 69 F. Fringuelli and A. Taticchi, *Dienes in the Diels–Alder reaction*, Wiley, 1990.
- 70 T. P. Vispute and G. W. Huber, *Green Chem.*, 2009, **11**, 1433–1445.
- 71 P. A. Wadsworth and D. C. Villalanti, *Hydrocarbon Process., Int. Ed.*, 1992, **71**, 109–112.
- 72 R. A. Bourne, J. G. Stevens, J. Ke and M. Poliakoff, *Chem. Commun.*, 2007, 4632–4634.
- 73 J. C. Serrano-Ruiz, D. Wang and J. A. Dumesic, *Green Chem.*, 2010, **12**, 574–577.
- 74 J. C. Serrano-Ruiz, D. J. Braden, R. M. West and J. A. Dumesic, *Appl. Catal., B*, 2010, **100**, 184–189.
- 75 L. A. Larson and J. T. Dickinson, *Surf. Sci.*, 1979, **84**, 17–30.
- 76 C. Fellay, P. J. Dyson and G. Laurenczy, *Angew. Chem., Int. Ed.*, 2008, **47**, 3966–3968.
- 77 B. J. O'Neill, E. I. Gürbüz and J. A. Dumesic, *J. Catal.*, 2012, **290**, 193–201.
- 78 M. Ojeda and E. Iglesia, *Angew. Chem., Int. Ed.*, 2009, **48**, 4800–4803.
- 79 X.-L. Du, L. He, S. Zhao, Y.-M. Liu, Y. Cao, H.-Y. He and K.-N. Fan, *Angew. Chem., Int. Ed.*, 2011, **50**, 7815–7819.
- 80 S. M. Sen, C. A. Henao, D. J. Braden, J. A. Dumesic and C. T. Maravelias, *Chem. Eng. Sci.*, 2012, **67**, 57–67.
- 81 H. J. Bart, J. Reidetschlager, K. Schatka and A. Lehmann, *Ind. Eng. Chem. Res.*, 1994, **33**, 21–25.
- 82 P. M. Ayoub, *World Pat.*, WO/2005/070867, 2005.
- 83 J. Q. Bond, D. Martin Alonso, R. M. West and J. A. Dumesic, *Langmuir*, 2010, **26**, 16291–16298.
- 84 J. Q. Bond, D. Wang, D. M. Alonso and J. A. Dumesic, *J. Catal.*, 2011, **281**, 290–299.
- 85 D. Mohan, C. U. Pittman and P. H. Steele, *Energy Fuels*, 2006, **20**, 848–889.
- 86 H. Zhang, T. R. Carlson, R. Xiao and G. W. Huber, *Green Chem.*, 2012, **14**, 98–110.
- 87 Y. C. Lin, J. Cho, G. A. Tompsett, P. R. Westmoreland and G. W. Huber, *J. Phys. Chem. C*, 2009, **113**, 20097–20107.
- 88 J. Cho, J. M. Davis and G. W. Huber, *ChemSusChem*, 2010, **3**, 1162–1165.
- 89 T. R. Carlson, J. Jae, Y.-C. Lin, G. A. Tompsett and G. W. Huber, *J. Catal.*, 2010, **270**, 110–124.
- 90 T. Q. Hoang, X. Zhu, T. Sooknoi, D. E. Resasco and R. G. Mallinson, *J. Catal.*, 2010, **271**, 201–208.
- 91 A. Corma, G. W. Huber, L. Sauvinaud and P. O'Connor, *J. Catal.*, 2007, **247**, 307–327.
- 92 M. Bjørgen, S. Svelle, F. Joensen, J. Nerlov, S. Kolboe, F. Bonino, L. Palumbo, S. Bordiga and U. Olsbye, *J. Catal.*, 2007, **249**, 195–207.
- 93 T. R. Carlson, J. Jae and G. W. Huber, *ChemCatChem*, 2009, **1**, 107–110.
- 94 A. J. Foster, J. Jae, Y. T. Cheng, G. W. Huber and R. F. Lobo, *Appl. Catal., A*, 2012, **423**, 154–161.
- 95 J. Jae, G. A. Tompsett, A. J. Foster, K. D. Hammond, S. M. Auerbach, R. F. Lobo and G. W. Huber, *J. Catal.*, 2011, **279**, 257–268.
- 96 T. R. Carlson, G. A. Tompsett, W. C. Conner and G. W. Huber, *Top. Catal.*, 2009, **52**, 241–252.
- 97 H. Y. Zhang, R. Xiao, B. S. Jin, D. K. Shen, R. Chen and G. M. Xiao, *Bioresour. Technol.*, 2013, **137**, 82–87.
- 98 A. Aho, N. Kumar, K. Eränen, T. Salmi, M. Hupa and D. Y. Murzin, *Fuel*, 2008, **87**, 2493–2501.
- 99 T. R. Carlson, T. R. Vispute and G. W. Huber, *ChemSusChem*, 2008, **1**, 397–400.
- 100 M. R. Apelian, W. K. Bell, S. L. A. Fung, W. O. Haag and C. R. Venkat, *EP Pat.*, 0 570 136, 1998.
- 101 M. Choi, H. S. Cho, R. Srivastava, C. Venkatesan, D.-H. Choi and R. Ryoo, *Nat. Mater.*, 2006, **5**, 718–723.
- 102 K. H. Park, H. J. Park, J. Kim, R. Ryoo, J.-K. Jeon, J. Park and Y.-K. Park, *J. Nanosci. Nanotechnol.*, 2010, **10**, 355–359.
- 103 H. J. Park, H. S. Heo, J.-K. Jeon, J. Kim, R. Ryoo, K.-E. Jeong and Y.-K. Park, *Appl. Catal., B*, 2010, **95**, 365–373.
- 104 T. Q. Hoang, X. Zhu, L. L. Lobban, D. E. Resasco and R. G. Mallinson, *Catal. Commun.*, 2010, **11**, 977–981.
- 105 Y. T. Cheng, J. Jae, J. Shi, W. Fan and G. W. Huber, *Angew. Chem., Int. Ed.*, 2012, **124**, 1416–1419.
- 106 J. M. Cho, S. Chu, P. J. Dauenhauer and G. W. Huber, *Green Chem.*, 2012, **14**, 428–439.
- 107 S. Chu, A. V. Subrahmanyam and G. W. Huber, *Green Chem.*, 2013, **15**, 125–136.
- 108 S. M. Sen, D. M. Alonso, S. G. Wettstein, E. I. Gurbuz, C. A. Henao, J. A. Dumesic and C. T. Maravelias, *Energy Environ. Sci.*, 2012, **5**, 9690–9697.
- 109 *Aspen Plus v7.3*, Aspen Technology, Inc., Cambridge, MA, 2011.
- 110 *Aspen Process Economic Analyzer v7.3.1*, Aspen Technology, Inc., Cambridge, MA, 2011.
- 111 J. M. Douglas, *AIChE J.*, 1985, **31**, 353–362.
- 112 J. M. Douglas, *Conceptual design of chemical processes*, McGraw-Hill, New York, 1988.
- 113 A. A. Upadhye, W. Qi and G. W. Huber, *AIChE J.*, 2011, **57**, 2292–2301.

- 114 H. Goyal, D. Seal and R. Saxena, *Renewable Sustainable Energy Rev.*, 2008, **12**, 504–517.
- 115 M. Pearlson, C. Wollersheim and J. Hileman, *Biofuels, Bioprod. Biorefin.*, 2013, **7**, 89–96.
- 116 D. C. Elliott, *Energy Fuels*, 2007, **21**, 1792–1815.
- 117 E. Furimsky, *Appl. Catal., A*, 2000, **199**, 147–190.
- 118 D. D. Laskar, B. Yang, H. M. Wang and J. Lee, *Biofuels, Bioprod. Biorefin.*, 2013, **7**, 602–626.
- 119 M. P. Pandey and C. S. Kim, *Chem. Eng. Technol.*, 2011, **34**, 29–41.
- 120 P. Azadi, O. R. Inderwildi, R. Farnood and D. A. King, *Renewable Sustainable Energy Rev.*, 2013, **21**, 506–523.
- 121 M. Wright, J. Satrio, R. Brown, D. E. Daugaard and D. Hsu, *Techno-economic analysis of biomass fast pyrolysis to transportation fuels*, Report TP-6A20–46586, NREL, 2010.
- 122 P. M. Mortensen, J. D. Grunwaldt, P. A. Jensen, K. G. Knudsen and A. D. Jensen, *Appl. Catal., A*, 2011, **407**, 1–19.
- 123 K. Kazi, J. Fortman, R. Anex, G. Kothandaraman, D. Hsu, A. Aden and A. Dutta, *Techno-economic analysis of biochemical scenarios for production of cellulosic ethanol*, Report TP-6A2–46588, NREL, 2010.
- 124 R. M. Swanson, J. A. Satrio, R. C. Brown, A. Platon and D. D. Hsu, *Techno-economic analysis of biofuels production based on gasification*, Report TP-6A20–46587, NREL, 2010.
- 125 J. Han, S. M. Sen, D. M. Alonso, J. A. Dumesic and C. T. Maravelias, *Green Chem.*, 2014, **16**, 653–661.
- 126 J. Kim, S. M. Sen and C. T. Maravelias, *Energy Environ. Sci.*, 2013, **6**, 1093–1104.